Journal of Petroleum Exploration and Production Technology (2023) 13:19–42
https://doi.org/10.1007/s13202-022-01531-z

ORIGINAL PAPER-PRODUCTION GEOPHYSICS

Predicting shear wave velocity from conventional well logs with deep and hybrid machine learning algorithms

Meysam Rajabi[1] · Omid Hazbeh[2] · Shadfar Davoodi[3] · David A. Wood[4] · Pezhman Soltani Tehrani[5] · Hamzeh Ghorbani[6] · Mohammad Mehrad[7] · Nima Mohamadian[8] · Valeriy S. Rukavishnikov[3] · Ahmed E. Radwan[10]

Received: 14 April 2022 / Accepted: 4 June 2022 / Published online: 11 July 2022

Abstract

Shear wave velocity (V_S) data from sedimentary rock sequences is a prerequisite for implementing most mathematical models of petroleum engineering geomechanics. Extracting such data by analyzing finite reservoir rock cores is very costly and limited. The high cost of sonic dipole advanced wellbore logging service and its implementation in a few wells of a field has placed many limitations on geomechanical modeling. On the other hand, shear wave velocity V_S tends to be nonlinearly related to many of its influencing variables, making empirical correlations unreliable for its prediction. Hybrid machine learning (HML) algorithms are well suited to improving predictions of such variables. Recent advances in deep learning (DL) algorithms suggest that they too should be useful for predicting V_S for large gas and oil field datasets but this has yet to be verified. In this study, 6622 data records from two wells in the giant Iranian Marun oil field (MN#163 and MN#225) are used to train HML and DL algorithms. 2072 independent data records from another well (MN#179) are used to verify the V_S prediction performance based on eight well-log-derived influencing variables. Input variables are standard full-set recorded parameters in conventional oil and gas well logging data available in most older wells. DL predicts V_S for the supervised validation subset with a root mean squared error (RMSE) of 0.055 km/s and coefficient of determination (R^2) of 0.9729. It achieves similar prediction accuracy when applied to an unseen dataset. By comparing the V_S prediction performance results, it is apparent that the DL convolutional neural network model slightly outperforms the HML algorithms tested. Both DL and HLM models substantially outperform five commonly used empirical relationships for calculating V_S from V_p relationships when applied to the Marun Field dataset. Concerns regarding the model's integrity and reproducibility were also addressed by evaluating it on data from another well in the field. The findings of this study can lead to the development of knowledge of production patterns and sustainability of oil reservoirs and the prevention of enormous damage related to geomechanics through a better understanding of wellbore instability and casing collapse problems.

Keywords Shear wave velocity · Hybrid machine learning · Deep learning · Well-log influencing variables · Multi-well dataset · Convolutional neural network

✉ Hamzeh Ghorbani
hamzehghorbani68@yahoo.com

Extended author information available on the last page of the article

Abbreviations

AAPD	Absolute average percent deviation
ACE	Alternative condition expectation
AE	Average error
AI	Artificial intelligence
ANFIS	Adaptive neuro-fuzzy inference
ANN	Artificial neural network
APD	Average percent deviation
BPANN	Backpropagation artificial neural network
Cal	Caliper log
CFBNN	Conventional feedforward backpropagation neural network
CFD	Cumulative distribution functions
CFM	Committee fuzzy machine
CMIS	Committee machine with intelligent systems
CNL	Compensated neutron
CNN	Convolutional neural network
COA	Cuckoo optimization algorithm
CP	Caliper
DL	Deep learning
DPHI	Density porosity
DT	Compressional wave slowness (delta T)
ELM	Extreme learning machine
ENN	Elman neural network
FFANN	Feedforward artificial neural network
FL	Fuzzy logic
GA	Genetic algorithm
Gb	Global position
GEP	Gene expression programming
GR	Gamma ray
GRG	Generalized reduced gradient
GRNN	General regression neural network
LSSVM	Least-squares support-vector machines
LSTM	Long short-term memory networks
MD	Wireline measured depth log
MELM	Multi extreme learning machine
MF	Memetic firefly
ML	Machine learning technique
MLP	Multi-layer perceptron
MSE	Mean squared error
n	The number of data points in the population
NARX	Nonlinear autoregressive network with exogenous inputs
NPHI	Neutron porosity
OFIS	Optimized fuzzy inference
ONN	Optimized neural network
OSVR	Optimized support vector regression
P	Percentage of data records with values in a distribution less than a specific data record
Pb	Personal position
PDi	Percent deviation for ith data record
PEF	Photoelectric absorption factor
PERM	Permeability log
PS	Pattern search algorithm
PSO	Particle swarm optimization
Qi	The value of data record i for input variable Q
$\overline{Q}$	The average of the input variable Q
R	The dataset of data records
RES-DEP	Deep resistivity
RES-MED	Medium resistivity
RES-SHT	Shallow resistivity
RHOB	Bulk density
RMSE	Root mean square error
RNN	Recurrent neutral network
RS	Shallow resistivity
RT	True resistivity
SD	Standard deviation
SFIS	Surgeon's fuzzy inference
SML	Single machine learning
SP	Spontaneous potential
SVM	Support vector machine
SVR	Support vector regression
Ti	The value of data record i for input variable T
$\overline{T}$	The average value of the input variable T
TOB	Transparent open box
Vi(t)	Current time period velocity
Vi(t + 1)	Nest time period velocity
V_P	Compressional-wave velocity
W	Weight vector
x	Data variable value range
X	The value of variable x in a specific data record
x_i^l	The value of attribute *l* for data record I
$xmax^l$	The maximum value of the attribute *l* among all the data records in the dataset
$xmin^l$	The minimum value of the attribute *l* among all the data records in the dataset

Introduction

Petroleum geomechanics forms a critical part of reservoir engineering and wellbore construction models (Rhett 1998; Bazyrov et al. 2017; Akbarpour and Abdideh 2020; Mohamadian et al. 2021). Interactions of stress fields with subsurface lithologies and the formed structures require a comprehensive understanding of the mechanical behavior of the lithologies associated with gas and oil fields. Such an understanding helps to overcome many problematic drilling and field development challenges and reduce operational costs (Hudson et al. 2005; Rajabi et al. 2022a).

The development of geomechanical models depends on the availability of reliable data from laboratory analysis.

This involves mechanical tests on wellbore core samples recovered from the subsurface sedimentary columns penetrated during gas and oil field exploration and development (Khoshouei and Bagherpour 2021; Miah et al. 2021). However, due to the high cost and time associated with wellbore coring operations, few oil or gas field wells are actually sampled by coring. This means that the availability of geomechanical measurements from cores is severely restricted. Consequently, estimates and extrapolations for these parameters have to be used. Many empirical relationships have been developed to compensate for this shortcoming based on the use of petrophysical well-log data (Eberhart-Phillips et al. 1989; Jørstad et al. 1999; Sohail et al. 2020). The basic input requirement for many geomechanical empirical relationships is shear wave velocity (V_S) (Ghorbani et al. 2021). Moreover, for cost reasons and the limited geomechanical considerations associated with many historical wells, most wellbore logging suites do not record V_S using the advanced and expensive dipole sonic log.

Due to subsurface heterogeneities, geomechanical variables commonly vary across gas and oil reservoir formations and along the wellbore profiles (especially in directional/horizontal wells). Consequently, V_S prediction is often required based on a few core measurements combined with well-log variables recorded continuously along the wellbore profiles. Machine learning (ML) methods provide an alternative method to make more reliable V_S predictions than those provided by empirical relationships (Ashraf et al. 2020; Vo Thanh et al. 2020; Ali et al. 2021; Thanh et al. 2022; Vo-Thanh et al. 2022).

The compaction of reservoir and consequential subsidence associated with the Ekofisk field (North Sea) caused a great deal of additional cost to the field owners, which could have been avoided by evaluating the potential behavior of subsurface formations to engineering operations by applying appropriate geomechanical studies (Dusseault 2011). That field case highlights the necessity of conducting careful geomechanical studies for effective field development, thereby preventing extra operational costs (Fourie and Vawda 1992). However, providing appropriate geomechanical studies requires geomechanical data from the sedimentary sections of interest. Such data can be obtained in two ways. The first method is to measure the required data through the time intensive and costly geomechanical laboratory experiments on the available core plugs. This method provides non-continuous geomechanical data (limited to some specific points distributed across the sedimentary section) (Stark et al. 2014). The second method provides geomechanical data indirectly from petrophysical data, from which valuable rock properties, including porosity, density, and shear/compressional velocity, can be usefully determined (Medetbekova et al. 2021). The latter method is cost-effective since it does not require time consuming experiments and provides a continuous geomechanical dataset across the logged section of a wellbore (Tokeshi et al. 2013). Among the petrophysical logs required for this method, V_S tends not to be routinely recorded in every well drilled in oil and gas fields, due to the additional operational cost associated with the specific logging tool required to record it (Wang et al. 2020). As a result, establishing predictive models for indirect evaluation of V_S can be very useful for conducting geomechanical studies. Additionally, V_S data is valuable for assisting decision-making in the selection of drilling locations and wellbore trajectories to ensure they achieve maximum well stability, preventing sand production, and the selection of appropriate zones for hydraulic fracturing (Fourie and Vawda 1992; Stark et al. 2014).

There are two conventional ways commonly used to estimate V_S. These are (i) predictive models based on rock physics, and (ii) empirical correlation-based relationships (Wang et al. 2019). Modeling methods use the physical properties of rocks to develop petrophysical models to predict V_S. Indeed, in rock physics modeling, V_S is obtained by studying different rock physics models to calculate rocks' effective elastic parameters. The factors that are typically considered in rock physics modeling are, porosity, pore shape, fluid inclusion properties, and matrix mineralogy (Wang et al. 2020). Several different physic-based models have developed for so far V_S estimation (Xu and White 1995; Sun et al. 2008; Zhang et al. 2012; Guo and Li 2015; Darvishpour et al. 2019; Zhang et al. 2020; Ali et al. 2021). Theoretically, the rock physics model-based methods are not limited in application to specific geographic areas or petroleum basins, because they adequately address many of the drawbacks of empirical equations. Nevertheless, most of the modeling methods based on rock physics involve very complicated estimation processes due to their need to make assumptions about the shape of pores. Such assumptions tend to reduce, to some degree, the validity of the estimation results. Besides, in such models the matrix elastic parameters, compositions, and the mixing mode must be taken into account, together with the effects of pore shapes and the fluid constituents, to achieve accurate V_S predictions. As a result of these difficulties,

Table 1 Published common empirical correlations used to predict shear wave velocity (V_S)

References	Proposed equations
(Pickett 1963)	$V_s = V_P/1.9$
(Coello et al. 2007)	$V_s = 1.09913326(V_p^{0.9238115636})$
(Castagna et al. 1985)	$V_s = 1.0168V_P - 0.05509V_p^2 - 1.0305$
(Eskandari et al. 2004)	$V_s = -1.1236V_p^2 + 1.61V_P - 2.3057$
(Brocher 2005)	$V_s = 0.7858 - 1.2344V_P + 0.7949V_p^2 - 0.1238V_p^3 + 0.0064V_p^4$

the models based on rock physics are of low efficiency and their complexity limits their appeal for real-world drilling and field development applications. The empirical correlation methods have been widely used to estimate V_S from compressional wave velocity (V_P) since they are quick and simple to apply, and relatively reliable methods (Wang et al. 2020) (Bailey and Dutton 2012; Lee 2013; Ojha and Sain 2014; Oloruntobi et al. 2019; Oloruntobi and Butt 2020). The reliability of empirical correlation equations originates from the fact that most of the factors affecting V_P also influence V_S in a similar manner but to different degrees (Xu and White 1995; Oloruntobi and Butt 2020). Table 1 lists some of the most commonly used empirical equations developed for V_S prediction involving various relationships with V_P. Vs signals recorded can be influenced by earthquake effects (Güllü and Pala 2014; Güllü and Jaf 2016; Güllü and Karabekmez 2017).

The fact that most empirical correlations for V_S prediction oy iolve V_P (Table 1) limits their accuracy and tends to make them field or basin specific. The results of these empirical equations are considerably influenced by lithology type, which may lead to inadequate prediction accuracy (Akhundi et al. 2014; Güllü and Jaf 2016). Besides, the lack of generalizability to other fields and their poor fit with real data across an entire sedimentary section limits the confidence with which such relationships can be applied (Güllü and Pala 2014; Güllü and Jaf 2016; Gholami et al. 2020; Oloruntobi and Butt 2020; Rajabi et al. 2021; Rajabi et al. 2022a). In recent years, the much-improved computational efficiency and prediction accuracy achieved by various ML methods has resulted in various ML methods being applied to predict V_S from well-log input data (Eskandari et al. 2004; Rezaee et al. 2007; Rajabi et al. 2010; Asoodeh and Bagheripour 2013, 2014; Gholami et al. 2014; Maleki et al. 2014; Oloruntobi et al. 2019; Gholami et al. 2020; Wang et al. 2020; Zhang et al. 2020). The datasets used in those models are typically verified with just a few core measurements and in some cases, include seismic data, with details listed in Table 2 (Al-Dousari et al. 2016). However, as ML and deep learning (DL) methods improve and more extensive datasets become available from around the globe, much scope remains to improve on V_S prediction accuracy (Wang et al. 2020; Wood 2020). Moreover, the possibility exists to make the methodologies more robust and generalizable within hydrocarbon fields and across sedimentary basins.

In this paper, three recently developed techniques are developed and evaluated to predict V_S for several wells drilled in a giant oil field with both carbonate and sandstone reservoirs using data from standard well logs (Fig. 1). These include two HML techniques: multi-hidden layer extreme learning machine hybridized with a particle swarm optimizer (MELM-PSO); and MELM hybridized with a genetic algorithm (MELM-GA). The third technique is the DL model convolutional neural network (CNN). The main novelty and features of this study are to develop, apply, and compare Vs predictions from these three techniques applied to a large multiple-well dataset from a giant oil field. The Vs prediction performance of the DL and HML algorithms is also compared, for the same dataset, with commonly used empirical Vs prediction models. Recent research has applied machine and deep learning algorithms, as robust computational tools to many engineering fields in order to solve a wide range of problems. Furthermore, full-scale comparison is performed between the hybrid machine learning models and a deep learning model. This identifies the most effective and accurate model for predicting the shear wave velocity. As a verification measure, we also address possible concerns about ensuring the integrity and repeatability of the proposed machine learning practical models by applying them to data from another well in the field. As a fast and very low-cost solution compared to other available methods, the technique involves only minor disadvantages. Execution constraints (appropriate computer system processing power) represent a constraint related to the number of data records and log variables that these models can process. Additionally, the quality of the recorded standard logs is important, and poor quality recorded log data will result in higher Vs prediction errors. The method's advantages outweigh their disadvantages, and the HML and DL models developed can be defined as reference classes or libraries for general use.

Methods

Work flow

A work flow diagram (Fig. 2) summarizes the sequence of construction and evaluation steps involved in applying the DL and HML algorithms to predict V_S and establish the prediction accuracy achieved. The process sequence begins with compiling a dataset and statistically assessing the value distribution of each of the component data variables. The maximum and minimum values for each data variable (attribute) are used to normalize the variable values so that they fall within the range of −1 and + 1. Normalization is achieved using Eq. (1) and is important because it avoids scaling biases in the learning processes adopted by the DL and HML algorithms (Kamali et al. 2022).

$$x_i^l = \left(\frac{x_i^l - x\min^l}{x\max^l - x\min^l} \right) * 2 - 1 \tag{1}$$

where:

x_i^l = the value of attribute l for data record i;

Table 2 ML techniques previously proposed for predicting V_S. See source references for ML technique abbreviations

Reference	Data description		ML techniques	Statistical evaluation parameters**				
	Data points	Input parameters		R2	RMSE	AAPD%	APD%	MSE
(Eskandari et al. 2004)	–	GR, RHOB, NPHI, RT, DT, and X and Y coordinates	ANN	0.972	–	–	–	–
(Rezaee et al. 2007)	637	NPHI, RHOB, GR, RT, and V_P	FL*, ANN, and ANFIS	0.946	–	–	–	0.051
(Rajabi et al. 2010)	3030	RHOB, RT, and NPHI	GA, FL*, ANFIS	0.951	–	–	–	0.0148
(Asoodeh and Bagheripour 2012)	–	RHOB, RT, NPHI, and V_P	ANN, ANFIS, and CMIS	0.893	–	–	–	0.0086
(Asoodeh and Bagheripour 2013)	–	RHOB, RT, NPHI, and V_P	ANFIS	0.937	–	–	–	0.0071
(Maleki et al. 2014)	–	RHOB, GR, DTCO, RT, CAL, and NPHI	SVR-GA* and BPNN-GA	0.97	26.68	–	–	–
(Gholami et al. 2014)	–	27 physical and geomechanical seismic attributes	MLP	0.98	–	–	–	AE ≅ 22
(Asoodeh and Bagheripour 2014)	–	RHOB, RT, NPHI, and V_P	ACE stimulated neural network	0.952	–	–	–	0.0063
(Akhundi et al. 2014)	–	RHOB, GR, RS, RT, and NPHI	ANN	0.95	–	–	–	–
(Bagheripour et al. 2015)	4055	RHOB, GR, PEF, DT, RT, RS and NPHI	SVR	0.971	0.0733	1.7595	–0.0567	–
(Al-Dousari et al. 2016)	59	V_P and core sample data (grain density, clay content, porosity, permeability, and the cementation exponent)	GRNN	–	–	–	6.91	–
(Singh and Kanli 2016)	–	GR, NPHI, ROHB, RT, and V_P	FFANN	0.999	–	–	–	–
(Behnia et al. 2017)	516	γ, n, and V_P	GEP and ANFIS*	0.963	135.35	–	–	–
(Mehrgini et al. 2019)	760	RT, ROHB, GR, NPHI, and V_P	ENN*, ENN-PSO, MLP, MLP-PSO	0.9143	0.0636	–	–	–
(Shiroodi et al. 2017)	–	27 physical and geomechanical seismic attributes	SFIS, ANFIS, OFIS, and CFM*					
	0.884	69.93	0.0328	–	–			
(Alkinani et al. 2019)	–	NPHI, RHOB, and V_P	CFBNN and NARX network*	0.996	–	–	–	–
(Ghorbani et al. 2021)	–	GR, V_P, RHOB, NPHI,						
CAL, Vs	LSSVM-GA	0.9813	0.411	–	–	–		
(Zhang et al. 2020)	–	RHOB, NPHI, RT, GR, DT, and PEF	LSTM	> 0.95	–	–	–	–
(Wood 2020)	1000	GR, RHOB, NPHI, DPHI, RT, and V_P	TOB, TOB-GRG*, and TOB-Firefly	0.999	11.08	0.1764	−0.0145	–
(Gholami et al. 2020)	–	6 physical and geomechanical seismic attributes	ONN, OFIS, OSVR, and CM*	0.923	78.21	0.0219	–	–
(Wang et al. 2020)	2369	RHOB, Cal, CNL, GR, DT, PERM, RS, RT, SP, and V_P	PSO-LSTM*, LSTM, and RNN	0.990	0.0917	0.0097	0.0170	–
(Olayiwola and Sanuade 2021)	–	CAL, MD, GR, ROHB, NPHI, and V_P	ANN, LSSVM*, and ANFIS	0.971	0.0892	–	–	–

Technique with best performance

**Statistical parameters for the technique of best performance*

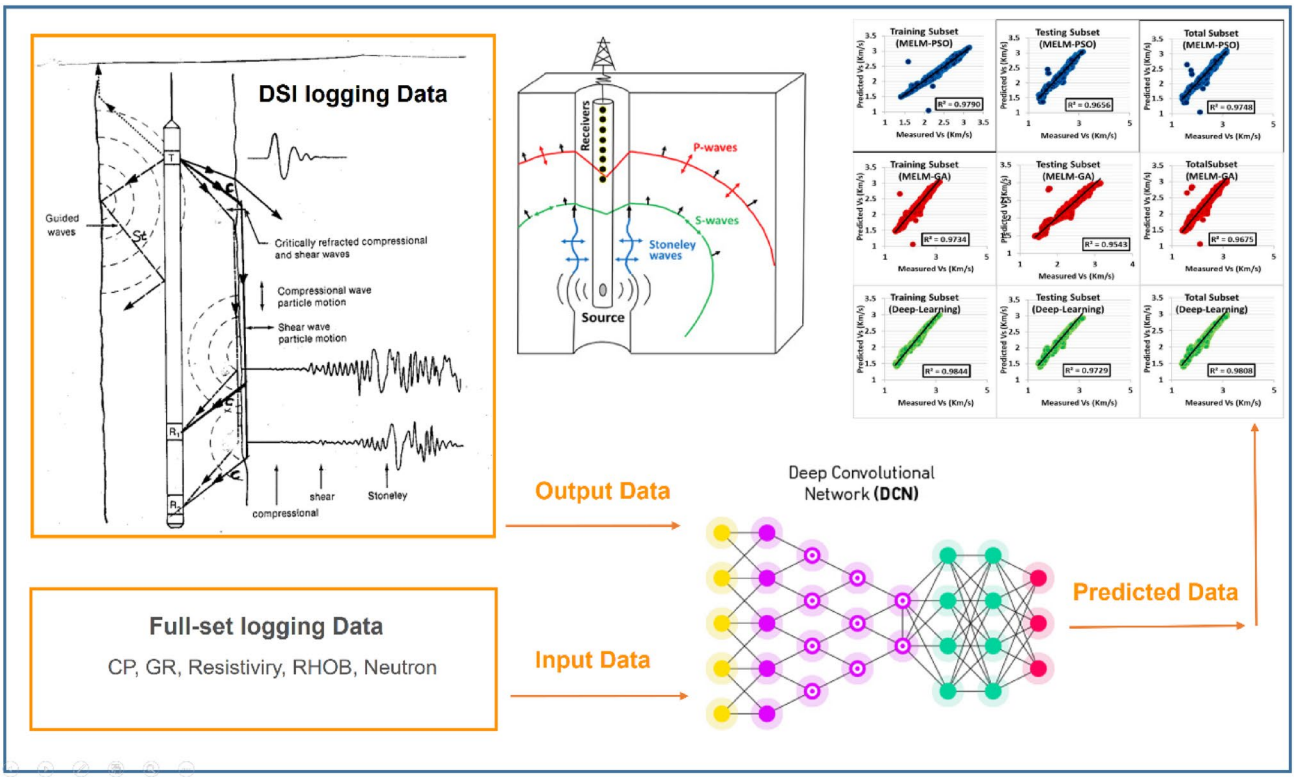

Fig. 1 Schematic diagram outlining the technique to predict Vs data from a standard suite of well logs by applying deep learning prediction model

$x\min^l$ = the minimum value of the attribute l. among all the data records in the dataset; and,

$x\max^l$ = the maximum value of the attribute l among all the data records in the dataset.

The normalized data records are then assigned to either a training subset or a testing subset. Trial and error tests indicate that an approximate 70%:30% split of data records between training and testing subsets works well for most reasonably sized datasets. The testing subset of data records is held independently of the training subset and is not involved in the algorithms' training processes. A K-fold method is used to sample the training subset for validation purposes. Statistical measures of accuracy are then used to assess the V_S prediction performance of each DL and HML algorithm evaluated to establish their relative V_S prediction capabilities.

Machine-learning (ML) algorithms

ML algorithms are now usefully applied to solve many oils and gas operational and prediction challenges including drilling, reservoir performance, and geomechanical characterization (Gullu 2017; Ashraf et al. 2020; Ashraf et al. 2021; Ranaee et al. 2021). ML algorithms are well suited to evaluating problems involving multiple variables with nonlinear relationships and complex value distributions (Gullu 2017; Hazbeh et al. 2021b). Recently, some researchers work on the shear wave velocity based on machine learning algorithms. Artificial neural network (ANN), extreme learning machine (ELM), support vector machine (SVM) and other algorithms based mainly on regression / correlation relationships have been successfully applied to progressively improve the prediction performance of variables relevant to the petroleum industry (Farsi et al. 2021b). Some of the researchers work on the *Vs* based on the ML work (Weijun et al. 2017; Azadpour et al. 2020; Zhang et al. 2020; Zhang et al. 2021; Miah 2021; Olayiwola et al. 2021; Zhong et al. 2021; Ebrahimi et al. 2022).

Single machine-learning (SML) algorithms

Extreme learning machine (ELM) ELM is a rapidly executed feed-forward neural network (Huang et al. 2006). It can be usefully applied to reduce learning time, improve accuracy, and increase generalizability (Huang et al. 2006; Huang et al. 2011; Huang 2014; Wang et al. 2014; Cheng and Xiong 2017; Naveshki et al. 2021; Zhang et al. 2022). ELM differs from an ANN, utilizing back-propagation or other optimization algorithms, in that all the ELM's internal

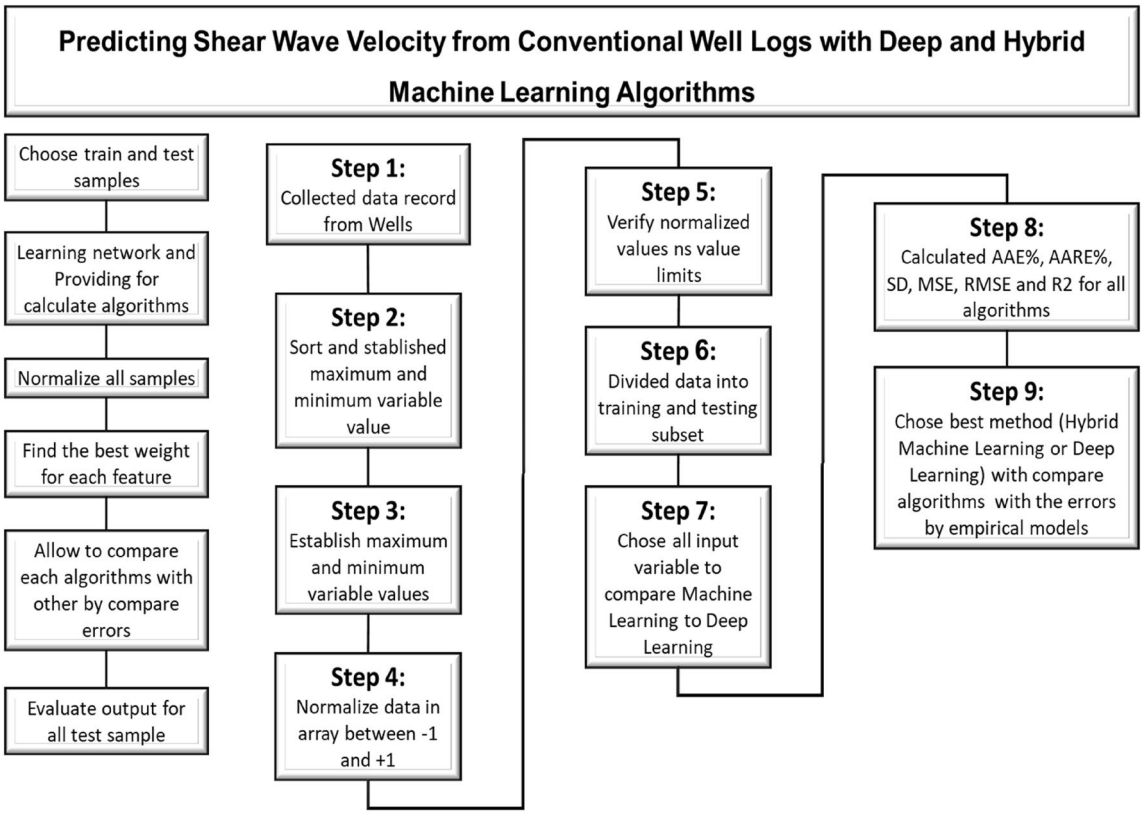

Fig. 2 Workflow schematic for comparing the V_S prediction performance of HML and DL algorithms

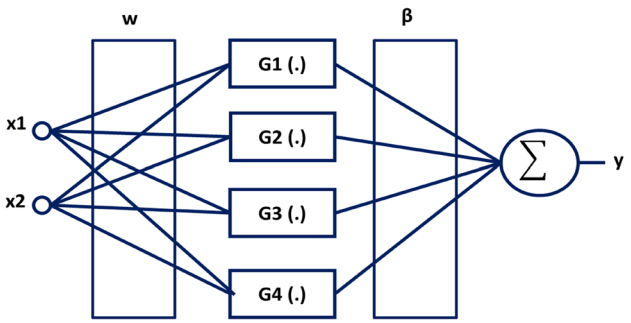

Fig. 3 *Schematic architecture of Extreme learning machine (ELM) with a single hidden layer. Modfied with permission from ref. (*Abad et al. 2021a*)*

learning parameters are randomly determined. This saves computational time as during ELM training, the parameters associated with the hidden layer (weights and biases) do not need to be adjusted. The output weights are determined by the inverse Moore–Penrose function applied to the hidden layer to output matrix (Yeom and Kwak 2017). The structure of a simple ELM (with a single hidden layer) is shown in Fig. 3.

ELM performance for complex problems can be improved by introducing more than one hidden layer. The multi-layer ELM algorithm is configured as follows:

Step 1: Determine the number of hidden layers (l) and neurons in each layer.
Step 2: Assuming $(X, Y) = (xi, y_i) = (i = 1,2, 3, \ldots, Q)$ as training data; where X is the matrix of input variable values for each data record and Y is the output variable vector including all data records.
Step 3: Each hidden layer has n neurons and an activation function g (x). Weights between layers i and (i-1) and biases applied to layer i are randomly generated.
Step 4: Calculate $W_{IE} = [B\ W]$, $X_E = [1\ X]^T$.
Step 5: Calculate the H matrix with Eq. (2):

$$H = g\left(W_{IE}X_E\right) \tag{2}$$

Step 6: If i is less than l, calculate Eq. (3) and return to step three. Otherwise go to the next step.

$$X = H^T, i = i + 1 \tag{3}$$

Step 7: The output weights are calculated based on the Moore–Penrose inverse by applying Eq. (4):

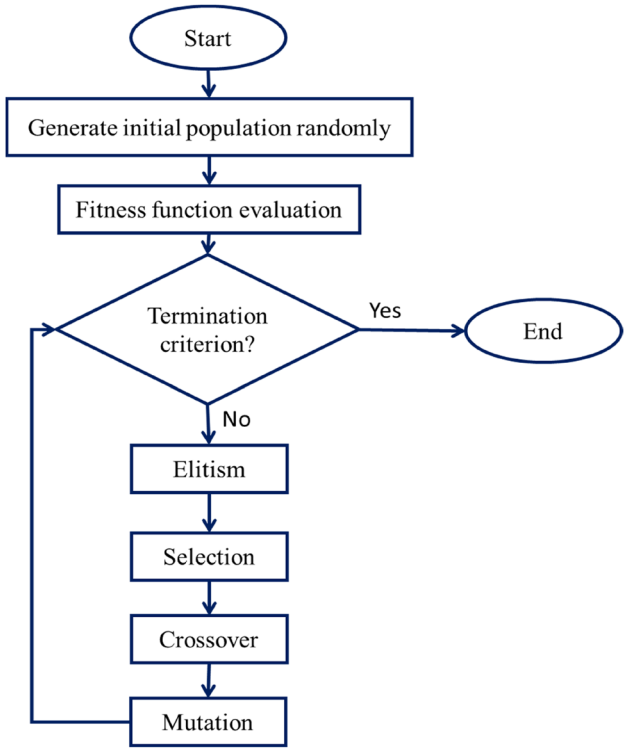

Fig. 4 Flowchart showing the execution sequence of a genetic algorithm (GA) optimizer

$$\beta = \text{pinv}\left(\text{H}^{\text{T}}\right) \times \text{Y} \tag{4}$$

Step 8: The output prediction is calculated with Eq. (5).:

$$\hat{Y} = \left(H^{T} \times \beta\right)^{T} \tag{5}$$

Genetic algorithm (GA) GA is an evolutionary algorithm developed in the 1960's and inspired by the principles of genetics, involving functions that mimic inheritance, mutation, selection, and combination. It establishes an initial population of randomly generated artificial "chromosomes" (Mohamadian et al. 2021). Each chromosome is evaluated through several evolutionary iterations with a cost function, which is progressively minimized. To determine the attributes of the next generation of "chromosomes" the value of the current generation is ranked (elitism) and only the best performing ones are "selected" to participate in reproduction. Crossover and mutation operations, with an assigned degree of randomness, are then involved in producing the next generation. The degree of randomness helps the GA from avoiding being trapped at local minima, enabling it to thoroughly explore the feasible solution space. Figure 4 illustrates the GA process in the form of a flowchart.

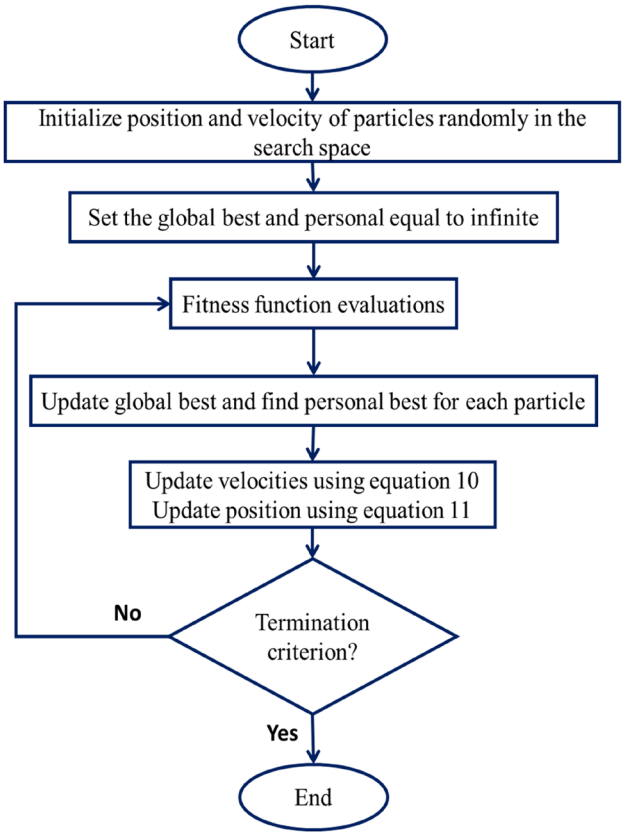

Fig. 5 Flowchart showing the execution sequence of a particle swarm optimizer (PSO). *Modfied with permission from ref. (*Rashidi et al. 2021*)*

Particle swarm optimization (PSO) algorithm Figure 5 illustrates the PSO algorithm in the form of a flowchart. PSO searches the feasible solution space using a population (swarm) of particles, the adjusted movements of which are inspired by those of flocks of birds or shoals of fish. The positions of the initial population are set randomly in the search space, which is defined by the minimum and maximum values of the decision variables. The particle is moved in different directions and at different speeds between the lower limit (V_{min}) and the upper limit (V_{max}) from one iteration to the next. The designated positions of each particle is recorded and their best historical individual position is stored as a "personal best" (P_b) and used in partially determining the movements going forward.

The position of all particles is evaluated by the objective function (cost function), and the particle with the lowest cost function value is identified in each iteration as the best global position (G_b). In each iteration, a new velocity (V_i (t + 1)) for each particle (i) is calculated based on the previous velocity (V_i (t)) and the distance of the

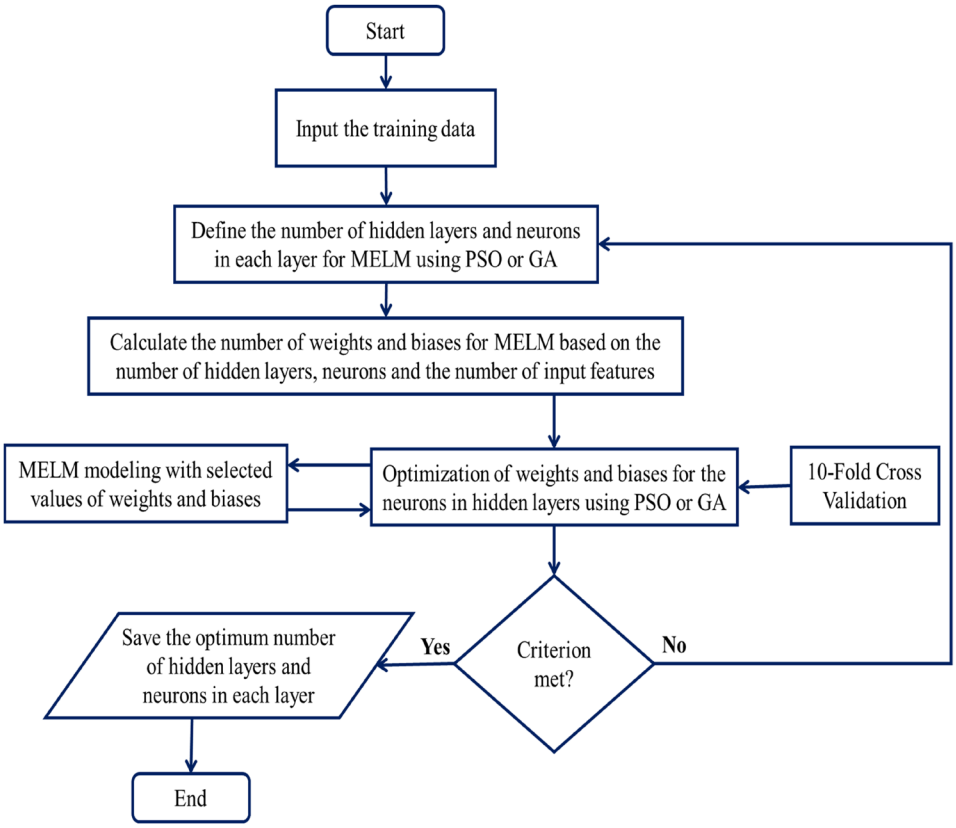

Fig. 6 Flowchart for implementing the hybrid MELM-PSO and MELM-GA applied to predict V_S. *Modfied with permission from ref. (*Abad et al. 2021a*)*

Table 3 GA control parameter values applied in the MELM-GA algorithm

Control Parameter	Value/Options
Number of iteration	200
Population	45
Selection method	Roulette wheel
Crossover	Uniform ($p=1$)
Mutation	Uniform ($p=0.05$)
Mutation rate	0.11
Selection pressure for Roulette wheel	2

Table 4 PSO control parameter values applied in the MELM-PSO algorithm

Control Parameter	Values
Number of iterations	200
Swarm size	40
Cognitive constant	2.05
Social constant	2.05
Interia weight (damping ratio)	0.96

particle's current position (x_i (t)) in the solution space compared to its best historical personal position and the best global position achieved by the swarm so far (Eq. 6). Subsequently, the new position of each particle (x_i (t + 1)) is calculated based on its prevailing position and the new calculated velocity (Eq. (7)).

$$V_i(t+1) = wV_i(t) + c_1r_1\left(Pb_i(t) - x_i(t)\right) + c_2r_2\left(G_b(t) - x_i(t)\right) \quad (6)$$

$$x_i(t+1) = x_i(t) + V_i(t+1) \quad (7)$$

where:

i = 1, 2, …, n, are the number of particles in the swarm;

w = Inertia weight, representing a recurrence value that controls particle velocity (Pedersen and Chipperfield 2010; Jafarizadeh et al. 2022);

c_1, c_2, are positive-valued personal (cognitive) and collective (social) learning coefficients, respectively (Coello et al. 2007); and,

r_1, r_2 are random numbers in the range [0,1].

The new position of each particle is then re-evaluated with the cost function. The PSO algorithm is well suited

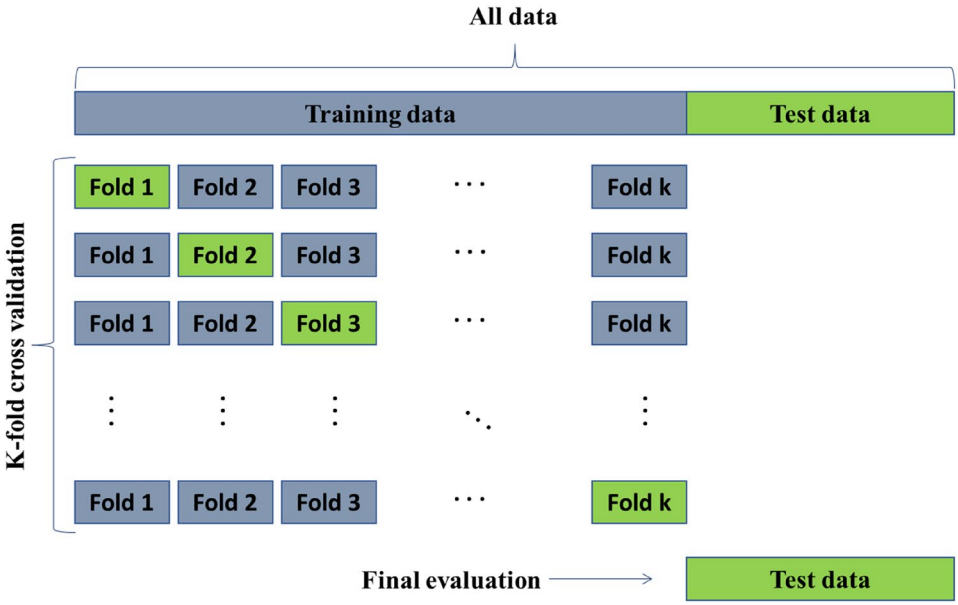

Fig. 7 K-fold cross-validation applied in the training phase (tenfold used) and values obtained then used to evaluate the testing subset

Table 5 The values of RMSE (V_S in km/s) for the different number of hidden layers and neurons in the layers for the MELM models developed for V_S prediction

Number of MELM hidden layer	Number of neurons in the MELM hidden layers				
	2	4	6	8	10
2	0.05341	0.05307	0.05129	0.04992	0.04998
4	0.05219	0.05286	0.05001	0.04900	0.04998
6	0.05224	0.05287	0.05013	0.04900	0.04997

to efficiently explore continuous solution spaces without becoming easily trapped at local minima.

HML algorithm configurations

Multi-layer extreme learning machine (MELM) hybridized with optimizers MELM performance depends on the number of hidden layers included, and the number of neurons in each of those layers. The MELM structure varies according to the complexities of the dataset (Rashidi et al. 2021). The more complex the problem, the greater the number of hidden layers and neurons. On the other hand, the more layers and neurons involved, the longer the computational time. Therefore, optimizing the MELM structure can lead to a high-precision model with an efficient learning process and relatively short computational requirements. A trial-and-error method can be used to determine the appropriate structures of multilayer ANN and MELM, but this can be very time consuming. Therefore, in this study the PSO algorithm is used to determine the number of MELM hidden layers and number of neurons in each layer. On the other hand, due to the process of randomly selecting of hyperparameters for MELM, different answers may be obtained each time the algorithm is implemented. To solve this problem, the MELM algorithm is combined with the optimizer (GA or PSO) to firstly identify the optimum hyperparameter values (Fig. 6).

GA and PSO optimization algorithms have adjustable hyperparameters (control values) that influence the efficiency of their performance. Trial-and-error methods were used to determine these control values (Tables 3 and 4). A total of 50 iterations of the optimizers were used to identify the optimum number of layers and neurons in the MELM, whereas 200 iterations (Tables 3 and 4) of the optimizers were used to optimize the weights and biases of the MELM-GA and MELM-PSO hybrid models (Abad et al. 2022).

The K-fold cross-validation technique was applied, with a tenfold set up, to achieve more stable and reliable V_S prediction results in determining the number of MELM layers and neurons. This divides the entire dataset into ten equal portions. The model is then evaluated ten times with each execution using nine portions of the data records as the training subset, and one portion of the data records as the validation subset (Fig. 7). Each of the ten portions is therefore used once as the validation subset.

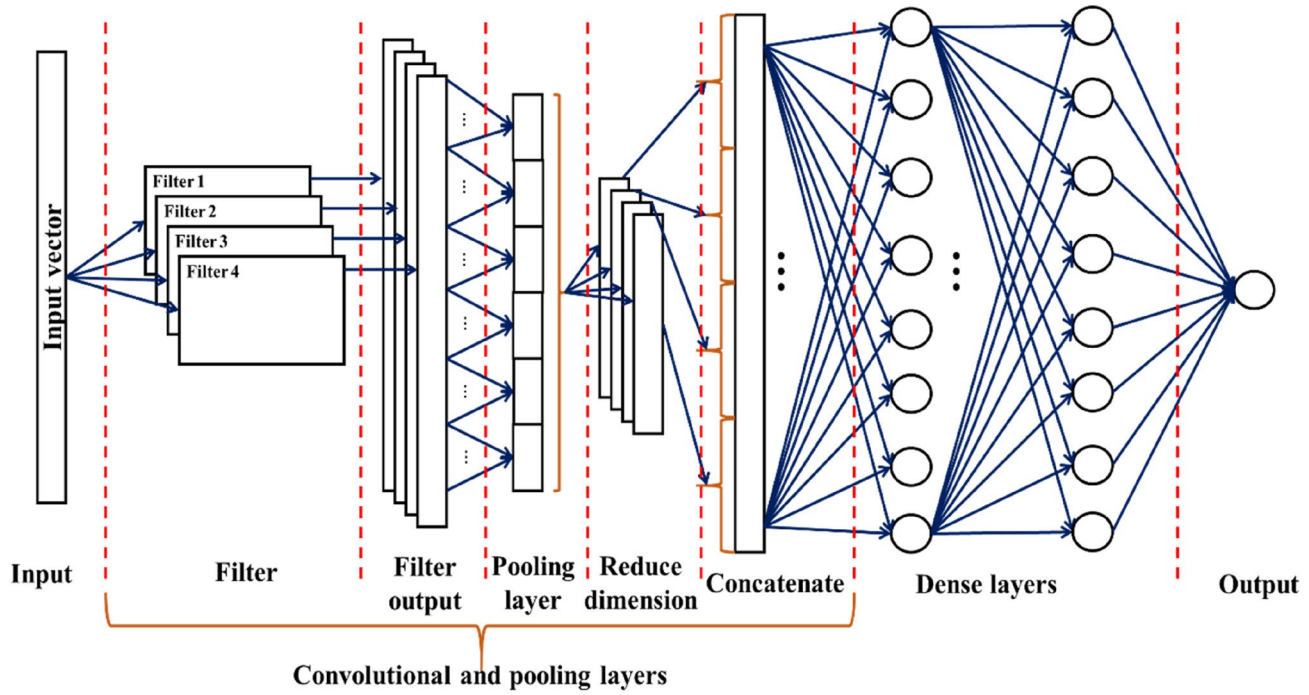

Fig. 8 Schematic illustration of the structure of a deep learning convolutional neural network (CNN). *Modfied with permission from ref. (*Abad et al. 2021b*)*

Table 5 shows the provisional V_S prediction results for different MELM structures, established by trial and error, using the tenfold cross-validation technique. They indicate that MELM with between 2 and 6 hidden layers and with between 6 and 10 neurons achieves the lowest RMSE for V_S predictions. In order to save computational time, the optimizers were therefore constrained to vary MELM layers between values of 2 and 6 and the number of neurons between 6 and 10.

Deep learning

Convolutional neural network (CNN)

CNN have demonstrated their capabilities in diverse applications in recent years, including prediction and learning applications related to image recognition (Krizhevsky et al. 2017), reading comprehension (Yu et al. 2018), and reinforcement learning in game strategy (Silver et al. 2016; Abad et al. 2021a). CNN uses convolutional (weight sharing) layers instead of the traditional fully connected layers of neural networks such as ANN and ELM (Abad et al. 2021b). This compresses the layers and neurons of CNN compared to fully connected networks and often enables them to generate higher resolution predictions with less training data records for specific problems.

Figure 8 shows a generic CNN structure. It has several parallel filters acting on the input data records that can be configured to extract different features. The input vector is filtered by each of the CNN filter layers, with each layer producing its own output vector; Therefore, the dimensions of the network increase with the number of filter layers selected. A pooling layer is then used to reduce the dimensions and normalize the selected variables, feeding that data into the concatenate layer. This information is then fed into the dense layer (s) to generate the final output. This dense layer (like the multilayer perceptron neural network) is made up of a number of neurons, the number of which is determined by the user (trial and error) or an optimizer. The model is executed to establish the weights and biases for the neurons in the dense layers that achieve the highest dependent variable prediction accuracy.

There are a number of hyperparameters that need to be set when developing a CNN model. For the CNN constructed in this study to predict V_S, based on trial-and-error, the number of filters was set to 200, A kernel size (convolutional window length) of 3 was selected, the "relux" activation function was applied and the number of neurons in the dense layer was set to 100.

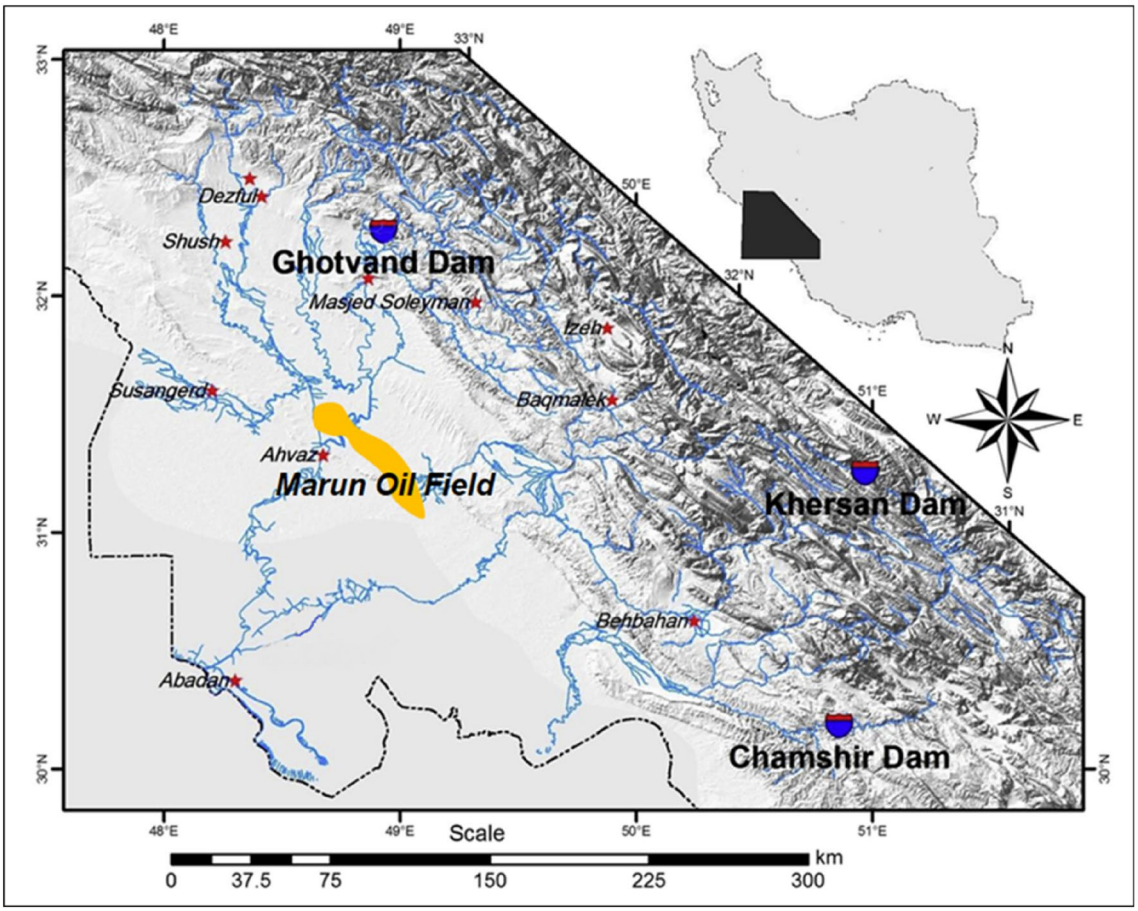

Fig. 9 Marun oil field located onshore Iran in the Zagros basin. Repoduced with permission from ref (Rashidi et al. 2020)

Statistical measures of prediction accuracy

V_S prediction performance comparison between the HLM, DL and empirical models evaluated are conducted by calculating widely used statistical measures of prediction accuracy as expressed in Eqs. 8, 9, 10, 11, 12, 13, 14 and 15.

Percentage deviation (PD) or relative error (RE)

$$\mathrm{PD}_i = \frac{H_{(\mathrm{Measured})} - H_{(\mathrm{Predicted})}}{H_{(\mathrm{Measured})}} x100 \tag{8}$$

Average percentage deviation (APD):

$$\mathrm{APD} = \frac{\sum_{i=1}^{n} PD_i}{n} \tag{9}$$

Absolute average percentage deviation (AAPD):

$$\mathrm{AAPD} = \frac{\sum_{i=1}^{n} |PD_i|}{n} \tag{10}$$

Standard Deviation (SD):

$$\mathrm{SD} = \sqrt{\frac{\sum_{i=1}^{n} \left(D_i - \mathrm{Dimean}\right)^2}{n-1}} \tag{11}$$

$$\mathrm{Dimean} = \frac{1}{n} \sum_{i=1}^{n} \left(H_{\mathrm{Measured}_i} - H_{\mathrm{Predicted}_i}\right) \tag{12}$$

Mean Square Error (MSE):

$$\mathrm{MSE} = \frac{1}{n} \sum_{i=1}^{n} \left(Z_{\mathrm{Measured}_i} - Z_{\mathrm{Predicted}_i}\right)^2 \tag{13}$$

Root Mean Square Error (RMSE):

$$\mathrm{RMSE} = \sqrt{\mathrm{MSE}} \tag{14}$$

Coefficient of Determination (R^2):

$$R^2 = 1 - \frac{\sum_{i=1}^{N} \left(H_{\mathrm{Predicted}_i} - H_{\mathrm{Measured}_i}\right)^2}{\sum_{i=1}^{N} \left(H_{\mathrm{Predicted}_i} - \frac{\sum_{i=1}^{n} H_{\mathrm{Measured}_i}}{n}\right)^2} \tag{15}$$

Table 6 Statistical characterization of the data variables constituting the well-log dataset for three Marun-oil-field wells: MN#163, MN#225 and MN#179

Field	Variables	Compressional-Wave Velocity	Gamma Ray	Bulk Density	Neutron	Shallow Resistivity	Medium Resistivity	Deep Resistivity	Caliper	Shear wave velocity
	Symbol (units)	V_P (km/s)	GR (API)	RHOB (g/cc)	NPHI (PU)	RES-SHT (Ohms-m)	RES-MED (Ohms-m)	RES-DEP (Ohms-m)	CP (Inches)	V_S (km/s)
3793 dataset records from MN#163	Mean	4.21	42.93	2.51	15.73	4.73	3.72	4.45	8.62	2.32
	Std. Deviation	0.58	61.77	0.12	10.07	89.47	2.63	51.42	0.04	0.33
	Variance	0.34	3815.10	0.01	101.30	8003.07	6.89	2643.24	0.00	0.11
	Minimum	2.71	1.04	2.16	3.28	0.20	0.19	0.23	8.47	1.40
	Maximum	5.19	316.27	2.93	54.65	5464.37	29.49	2189.60	8.87	3.15
2829 dataset records from MN#225	Mean	4.21	56.23	2.56	14.77	3.84	25.50	3.85	8.63	2.32
	Std. Deviation	0.46	60.24	0.07	8.45	2.79	908.59	3.05	0.03	0.30
	Variance	0.21	3627.25	0.00	71.32	7.79	825,241.98	9.33	0.00	0.09
	Minimum	2.72	5.67	2.21	4.23	0.71	0.14	0.70	8.50	1.46
	Maximum	5.09	587.02	2.70	54.35	14.34	46,224.45	15.07	8.77	2.94
2072 dataset records from MN#179	Mean	4.25	50.44	2.51	14.86	3.38	3.67	3.41	8.60	2.35
	Std. Deviation	0.58	88.41	0.11	10.58	2.32	2.60	2.49	0.04	0.30
	Variance	0.33	7812.47	0.01	111.93	5.37	6.75	6.21	0.00	0.09
	Minimum	2.62	4.16	1.98	2.90	0.55	0.47	0.61	8.52	1.43
	Maximum	5.41	410.44	2.66	59.32	13.36	31.32	14.08	8.75	2.87

These indicators of prediction accuracy are best considered together rather than individually as they all reveal complementary information and insight into the prediction performance of the algorithms considered. RMSE is used as the objective function for the HML and DL models, making it the single most important measure, as those algorithms are configured to minimize RMSE.

Data collection and characterization

Marun field description

To predict V_S, well log data from three wellbores drilled in the Marun oil field: MN#163, MN#225 and MN#179, are evaluated. This giant oil field is located onshore southwest of Iran (Fig. 9). It was discovered in 1963 and is one of the largest oil fields in the Zagros Basin with two producing oil reservoirs; the Asmari (Oligocene to Early Miocene) and Bangestan (Upper Cretaceous) formations. Collectively, these reservoirs contain in-place oil resources of some 46 billion barrels. In addition, the Khami (Lower Cretaceous) formation forms an underlying natural gas reservoir with some 462 trillion cubic feet of gas-in-place.

Data collection and data distribution

Well-log datasets compiled for wells MN#163, MN#225 and MN#179 sample the Asmari carbonate reservoir. Data records from two of the wells (MN#163 and MN#225) were used for supervised training and validation of the DL and HML algorithms in terms of V_S prediction accuracy. Data from well MN#179 was then used as an independent testing subset to test the models for V_S prediction accuracy with data previously unseen by the trained and validated model.

The well-log variables used as input features for the V_S prediction models are gamma ray (GR); compressional-wave velocity (V_P); bulk density (RHOB); neutron porosity

Table 7 V_S Prediction accuracy statistics for the training subset (~70% of available data records) in respect of shear wave velocity (V_S; km/s) (for MN#163 and MN#225)

Models	APD (%)	AAPD (%)	SD (STBD)	MSE (STBD)	RMSE (STBD)	R^2
Empirical models						
Pickett	4.286	5.099	6.524	0.025	0.159	0.8604
Carroll	−79.286	79.286	78.080	3.372	1.836	0.8608
Castagna et al	2.596	4.170	5.769	0.018	0.134	0.8605
Eskandari et al	2.902	4.577	6.662	0.021	0.143	0.8605
Brocher	−4.149	7.775	9.036	0.042	0.205	0.8607
Hybrid machine learning-optimizer models						
MELM-PSO	−0.331	1.562	2.373	0.002	0.048	0.9790
MELM-GA	−0.109	1.518	2.491	0.003	0.051	0.9734
Deep-Learning Model						
CNN	−0.025	1.337	1.951	0.002	0.041	0.9844

Table 8 V_S Prediction accuracy for the validation subset (~30% of available data records) in respect of shear wave velocity (V_S; km/s) (for MN#163 and MN#225)

Models	APD (%)	AAPD (%)	SD (STBD)	MSE (STBD)	RMSE (STBD)	R^2
Empirical models						
Pickett	4.037	4.923	6.307	0.023	0.153	0.8744
Carroll	−79.739	79.739	78.522	3.401	1.844	0.8747
Castagna et al	2.374	4.007	5.609	0.017	0.129	0.8729
Eskandari et al	2.719	4.428	6.568	0.019	0.140	0.8608
Brocher	−4.398	7.814	9.113	0.042	0.206	0.8735
Hybrid machine learning-optimizer models						
MELM-PSO	−0.562	2.082	3.113	0.004	0.062	0.9656
MELM-GA	−0.267	1.920	3.502	0.005	0.069	0.9543
Deep-Learning Model						
CNN	−0.103	1.804	2.616	0.003	0.055	0.9729

Table 9 V_S Prediction accuracy for all data records from wells MN#163 and MN#225, considered collectively

Models	APD (%)	AAPD (%)	SD (STBD)	MSE (STBD)	RMSE (STBD)	R^2
Empirical models						
Pickett	4.211	5.046	6.459	0.025	0.157	0.8646
Carroll	−79.422	79.422	78.207	3.380	1.839	0.8650
Castagna et al	2.530	4.121	5.721	0.018	0.132	0.8643
Eskandari et al	2.847	4.533	6.634	0.020	0.142	0.8537
Brocher	−4.224	7.787	9.059	0.042	0.205	0.8646
Hybrid machine learning-optimizer models						
MELM-PSO	−0.400	1.718	2.617	0.003	0.053	0.9748
MELM-GA	−0.157	1.639	2.832	0.003	0.057	0.9675
Deep-Learning Model						
DL	−0.048	1.477	2.171	0.002	0.046	0.9808

(NPHI); shallow resistivity (RES-SHT); medium resistivity (RES-MED); deep resistivity (RES-DEP) and caliper (CP). Table 6 statistically summarizes the distributions of the nine variables involved (8 input plus V_S as dependent variable) sampled from the Asmari reservoir sections penetrated by the three wells: MN#163 (3793 data records), MN#225 (2829 data records) and MN#179 (2072 data records), constituting 8694 data records in total.

The ranges of the data variables covered by the Asmari reservoir well-log samples are substantial (Table 6). For instance, the V_S range evaluated extends from 1.40 km/s to 3.15 km/s across the three wells considered. This highlights the lithological variety within the Asmari reservoir including, limestone, dolomite, shale, siltstone, sandstone and evaporite layers.

The best subset of input variables was selected based on evaluation of correlation coefficients between each input variables and the measured V_S values. The input variables displaying the highest correlation coefficients were selected for V_S modeling. Figure 13 shows that four input variables, V_P, GR, RHOB, and NPHI, have the highest correlation coefficients with V_S. The HML and DL model were initially built using these four selected features. The impact of the other potential input variables was then evaluated by adding them, one at a time, to the selected feature subset to predict V_S. The result of that analysis revealed that by adding the variables RES-DEP and RES-SHT, to the four originally selected features based on correlation coefficient, generated more accurate V_S predictions. Therefore, these six features were used to build the HML and DL models finally evaluated.

Results

Identifying the best performing algorithm for *VS* prediction

Tables 7 and 8 display the V_S prediction accuracies based on the training (70%) and validation (30%) subsets, respectively, selected from the 6622 data records available for wells MN#163 and MN#225. This represents the supervised training and learning performance for the HML and DL algorithms. The performance of five empirical relationships used for predicting V_S from V_P (Table 1) are also shown for each of these data subsets.

Table 9 displays the V_S prediction accuracies for the supervised and trained HML and DL algorithms applied to all 6622 data records for wells MN#163 and MN#225. The performance of five empirical relationships (Table 1) are also shown for comparison.

Close inspection of the models' V_S prediction results (Tables 7, 8 and 9) reveals that the DL CNN model achieves exceptionally high V_S prediction accuracy when applied to the two subsets and all data records for the two wells involved in supervised learning. (e.g., from Table 9 CNN: RMSE = 0.0456 km/s; AAPD = 1.477%; R^2 = 0.9808). The HML models also achieve high V_S prediction accuracy, for the two subsets and full supervised learning dataset, but they do not match that of the CNN model. The MELM-PSO model performs slightly better than the MELM-GA model. The recorded V_S prediction performance (RMSE) therefore ranks the DL, HML models and empirical equations as follows: CNN > MELM-PSO > MELM-GA > Castagna et al. > Eskandari et al. > Pickett > Brocher > Carroll.

It is very clear from Tables 7, 8 and 9 that the DL and HML models substantially outperform all five of the empirical models used to predict V_S using relationships with V_P. This outcome highlights the value of using information from

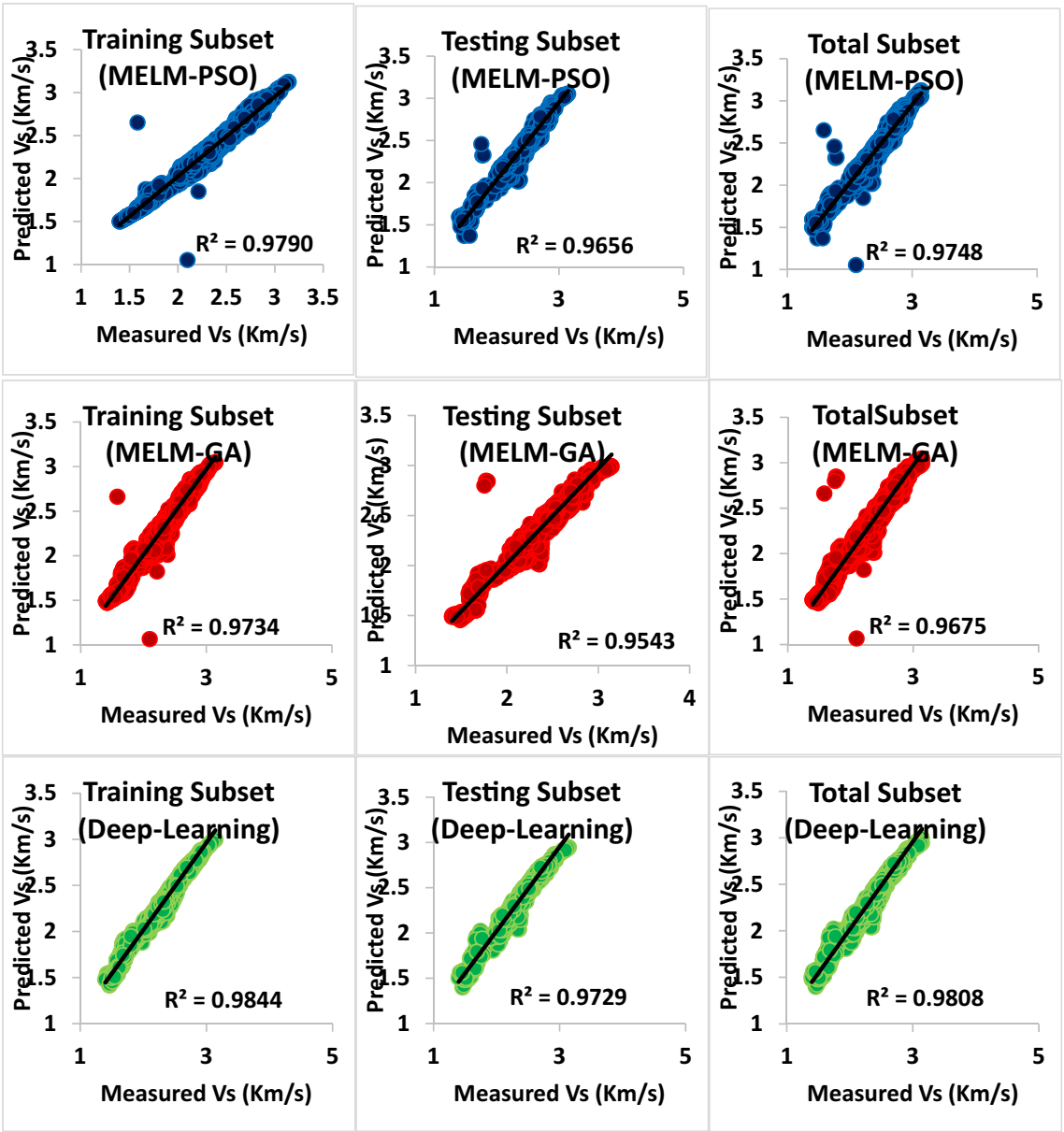

Fig. 10 Shear wave velocity (V_S) prediction versus measured values for each data record in the training and validation subsets and the full dataset evaluated for the Marun oil field wellhead measurements related to the 6622 data records from Marun oil field (for MN#163 and MN#225)

a suite of well logs rather than just relying on V_P data to predict V_S. Figure 10 displays the predicted versus measured V_S values for the data records in each subset and the full supervised learning dataset evaluated by the HML and DL models. The superior prediction performance of the DL CNN model is apparent as it involves no substantial outlier predictions. On the other hand, MELM-PSO and MELM-GA models do involve a few substantial outliers (only about 5 data records out of 6622 total data records).

Figure 11 reveals that the most commonly used empirical models (Table 1) provide workable V_S prediction accuracy ($R^2 \sim 0.86$) for this dataset but are substantially less reliable than the DL and HML models. The results in Table 1 show that the RMSE for an empirical equation is substantially greater than the RMSE for the CNN and HML models. The Castagna et al. (1993) relationship performs better than the other empirical models evaluated for the Asmari reservoir (Tables 7, 8 and 9). Figure 12 displays the relative percentage error (PD%) for V_S predictions for each of the 6622 data records (wells MN#163 and MN#225) constituting the training and validation subsets. These are displayed sequentially for the high performing DL and HML models. The PD% range for DL model ($\sim -20\% < \text{PDi} < \sim 15\%$) is substantially

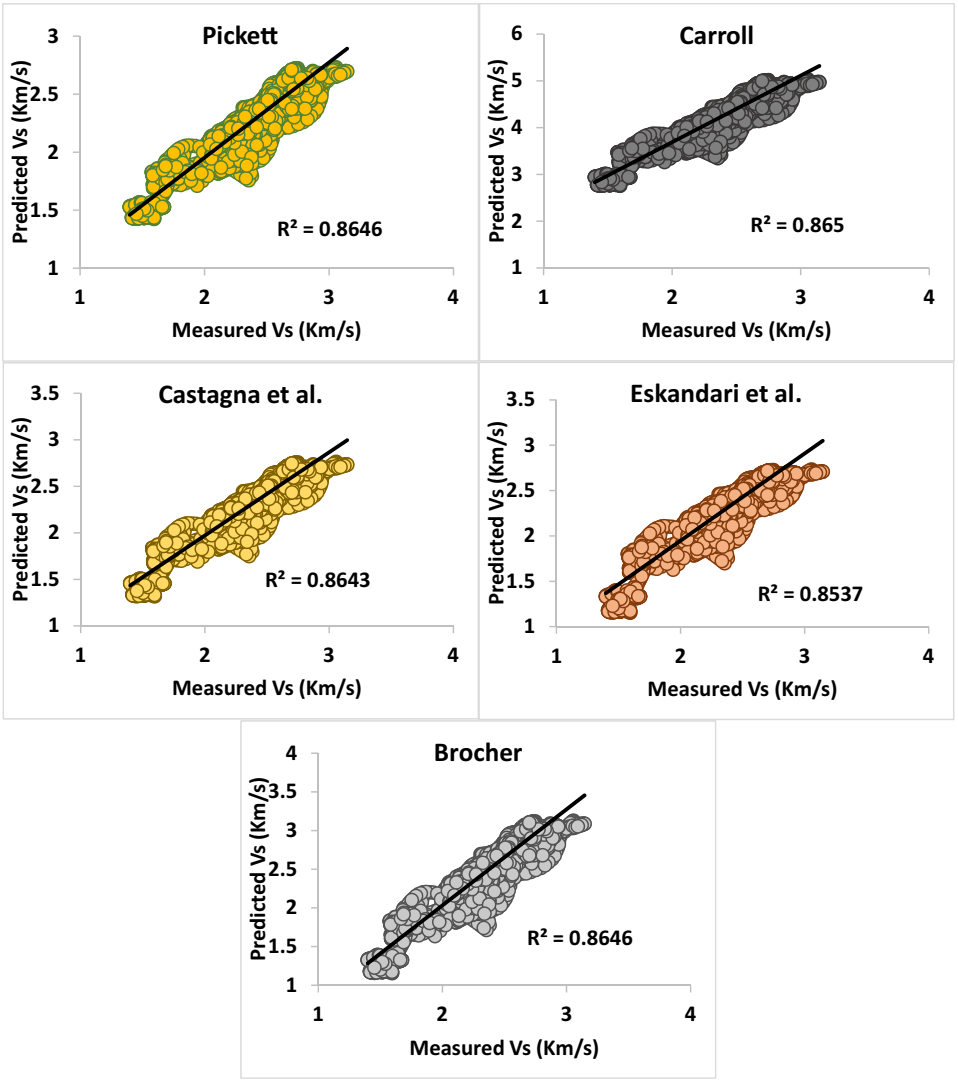

Fig. 11 V_S predicted versus V_S measured for the five empirical models applied to the full set of supervised learning data records (i.e., for wells MN#163 and MN#225)

better than for the HML models (~ -70% < PDi < ~ 45%) but for most data records PD% is < ± 5%. The PD% range for the empirical relationships is much greater, and for most data records PD% is > ± 15%. The Castagna et al. (1993) model performs better (~ −20% < PDi < ~ 25%) than other empirical models and the Carroll (1969) relationship performs the worst for the PD accuracy measure (~ −120% < PDi < ~ −20%).

A plot of V_S RMSE versus iteration number (Fig. 13) for the DL and HML algorithms identifies that all three algorithms converge to highly accurate solutions rapidly. The MELM-PSO and MELM-GA models converge at similar rates and after fewer iterations than the CNN algorithm. Although it takes more iterations, the CNN does achieve the lowest RMSE solutions by outperforming the HML algorithms after 100 iterations.

Discussion

Relative influences of the input variables on *VS*

Spearman's correlation coefficient (ρ), expressed on a scale of −1 to +1 (Gauthier 2001), is calculated (Eq. 16) to establish the nonparametric relationships between the input variables and V_S.

$$\rho = \frac{\sum_{i=1}^{n}\left(T_i - \overline{T}\right)\left(Q_i - \overline{Q}\right)}{\sqrt{\sum_{i=1}^{n}\left(T_i - T\right)^2 \sum_{i=1}^{n}\left(Q_i - \overline{Q}\right)^2}} \tag{16}$$

where:

$T_i = T$ input variable value of data record i;
$\overline{T}$ = mean value for variable T;
$Q_i = Q$ dependent variable (V_S) value of data record i;
$\overline{Q}$ = mean value for dependent variable Q;

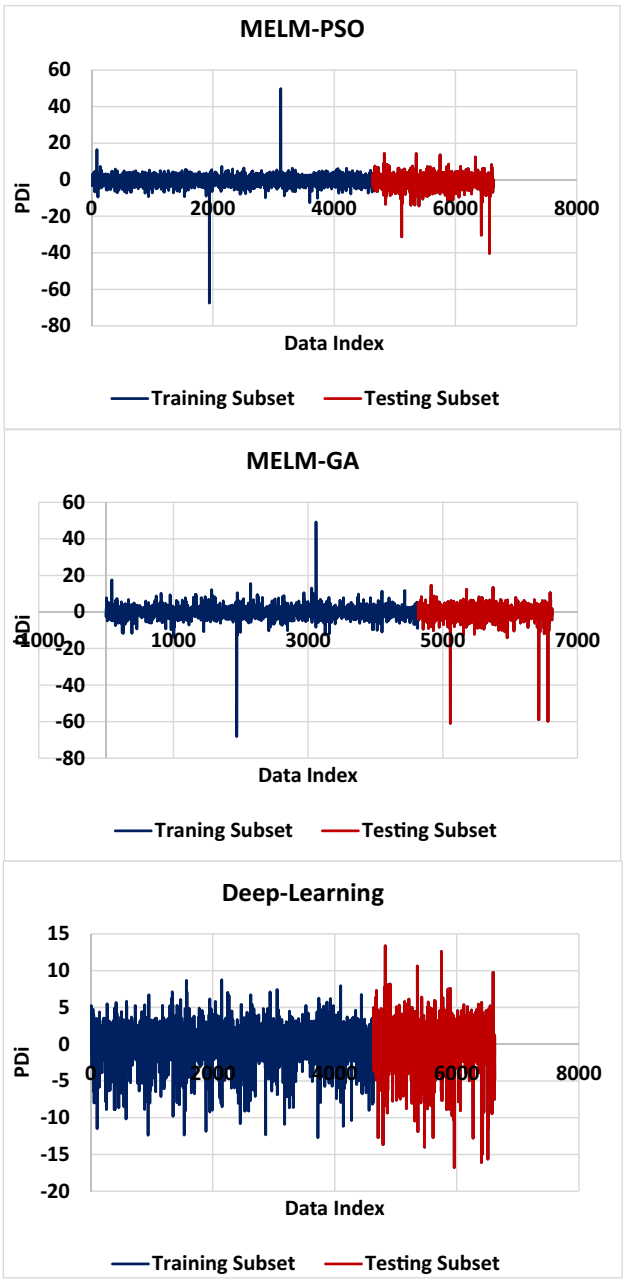

Fig. 12 V_S prediction error (PD%) compared for all 4635 training subset data records and 1987 validation subset data records for the DL and HML models evaluated (for wells MN#163 and MN#225)

n = number of data records in dataset or subset.

Figure 14 identifies, using the ρ values calculated for all 6622 of the supervised learning datasets, that V_P has, as should be expected, the greatest influence on V_S. On the other hand, *CP* has the least influence on V_S. The input variables NPHI, GR and RHOB also show substantial influences on V_S, whereas the resistivity variables show negligible influences on V_S.

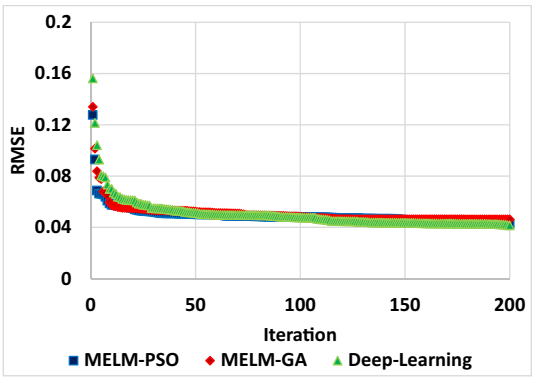

Fig. 13 V_S RMSE for the training subset (drawn from wells MN#163 and MN#225) for the DL and HML algorithms during supervised learning

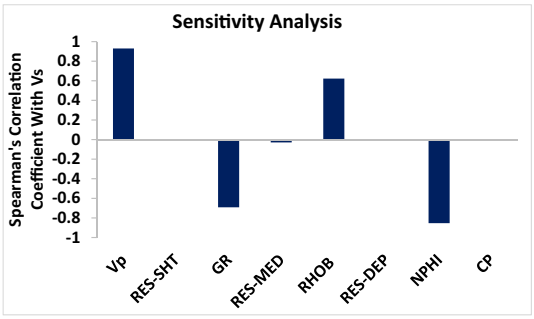

Fig. 14 V_S relationships with input variables assessed based on Spearman's non-parametric correlation coefficient values calculated for all data records of the supervised learning dataset (from wells MN#163 and MN#225)

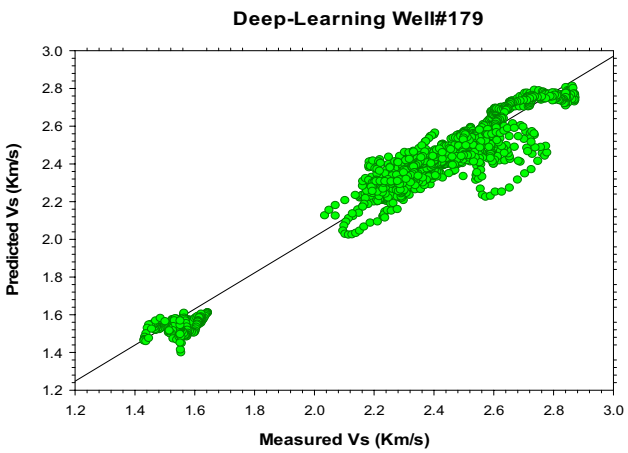

Fig. 15 Cross plot of predicted versus measured V_S values for the DL CNN model trained with data from wells MN#163 and MN#225 and applied to data records from well MN#179 previously unseen by the trained and validated model

Table 10 V_S prediction accuracy of the CNN model (trained with MN#163 and MN#225 dataset), applied to the Asmari reservoir section of Marun Field well MN#179 previously unseen by the trained and validated model

Models	APD (%)	AAPD (%)	SD (STBD)	MSE (STBD)	RMSE (STBD)	R2
DL (CNN)	−0.010	2.107	2.858	0.005	0.068	0.9675

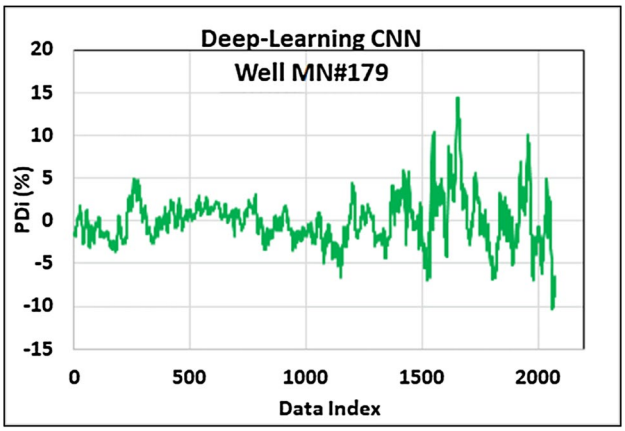

Fig. 16 V_S prediction error (PD%) for the DL CNN model trained with data from wells MN#163 and MN#225 and applied to data records from well MN#179 previously unseen by the trained and validated model

Development and generalization of CNN model applied to other marun field wells

The best V_S prediction model (DL CNN) established for the Asmari reservoir, trained based on supervised learning using the dataset compiled from wells MN#163 and MN#225, is applied to data previously unseen by the trained and validated model. It does so by evaluating the dataset compiled for Marun oil field well MN#179 (2072 data records; Tables 7, 8 and 9).

The statistical measures of accuracy achieved for these MN#179 data records using the same eight well-log data input variables are listed in Table 8. These results confirm high V_S prediction accuracy using the prediction model trained and validated with data from the other two wells. Figure 15 plots the measured versus predicted V_S values predicted by the CNN model trained with MN#163 and MN#225 data records and applied to all 2072 data records from wells MN# 179. The prediction performance is very good, confirming its reliability. This makes it suitable for application in other wells drilled into the Asmari reservoir in the Marun oil field for which V_S well log data has not been recorded. To apply the trained model to other wells, a standard suite of well logs is required for the wells of interest. Fortunately, such a suite of well logs is available for most of the existing wells in the field (Table 10).

Figure 16 shows the V_S prediction performance of the DL CNN model applied to the dataset from well MN#179 in terms of percentage error (PD%) for each data record arranged in order of sample depth through the Asmari reservoir. While most of the PD errors for these data records are is $< \pm 5\%$ in the lower 500 samples (equivalent to the lower 100 m of the Asmari section) several PD errors of between 5 and 15% are recorded. These outlying values in the lower part of the Asmari section drilled in well MN#179 are worthy of further analysis, but their prediction accuracy remains within reasonable error limits. The DL CNN model described and evaluated here could be used in a similar way to predict V_S in other fields but, of course, it would need to initially be recalibrated with some direct V_S measurements from at least one well in each of the fields / reservoirs to which it is applied.

Recommendations for future research works

Evaluation of the effect of the inclusion of other drilling parameters such as standpipe pressure and mud flow rate as input parameters along with well logging to predict V_S can be further investigated. According to the current findings, adding more related input parameters could provide models with higher prediction efficiencies. Involving other optimizers, such as genetic algorithms and firefly algorithms, in the development of a high-performance hybrid predictive model for V_S prediction can also be considered in future research work (Choubin et al. 2019; Ghorbani et al. 2020b; Kalbasi et al. 2021; Mohamadian et al. 2022; Rajabi et al. 2022b). The application of the proposed method should be investigated in a wide range of applications, e.g., various energy, ecological and natural research applications (Ghorbani et al. 2017; Ghorbani et al. 2019; Taherei Ghazvinei et al. 2018; Ahmadi et al. 2020; Band et al. 2020a; Band et al. 2020b; Emadi et al. 2020; Lei et al. 2020; Shamshirband et al. 2020; Barjouei et al. 2021; Hazbeh et al. 2021a). From computational fluid, pressure and hydrological modeling to environmental simulation for instance (Ghalandari et al. 2019b; Rezakazemi et al. 2019; Seifi et al. 2020; Farsi et al. 2021a; Mahmoudi et al. 2021) the proposed methodology can be effective. For the future research the comparative analysis with other machine learning methods, e.g., (Asadi et al. 2019; Ghalandari et al. 2019a; Ghorbani et al. 2020c; Joloudari et al. 2020; Mosavi et al. 2020; Sadeghzadeh et al. 2020; Shabani et al. 2020; Abdali et al. 2021; Mosavi and

Safaei-Farouji 2021) would be essential to bring an insight into the true potential of the proposed method. To improve the accuracy and the performance of the proposed method further deep learning, ensemble and hybrid methods for instance, those suggest in (Band et al. 2020b; Dehghani et al. 2020; Ghorbani et al. 2020a; Mosavi et al. 2020; Nabipour et al. 2020; Mousavi et al. 2021; Shamsirband and Mehri Khansari 2021) can come to the consideration.

Summary and conclusions

A large dataset of well-log data records compiled for the Asmari reservoir section penetrated by three Marun oil field wells (MN#163, MN#225 and MN#179) onshore Iran is compiled to predict shear wave velocity (V_S). The performances of two hybrid machine learning prediction models (MELM-PSO and MELM-GA), one deep learning model (CNN), and commonly used empirical models to predict V_S are compared using the compiled dataset. For supervised training of the MELM-PSO, MELM-GA, and CNN models data from two wells (MN#163 and MN#225; 6622 data records split 70%:30% between training and validation subsets) were initially evaluated. To independently test the best-performing trained model (CNN), 2072 data records of MN#179 previously unseen by the trained and validated model were also evaluated.

- The recorded V_S prediction performance (RMSE) ranks the DL, HML models and empirical equations as follows: (Best) CNN > MELM-PSO > MELM-GA > Castagna et al. > Eskandari et al. > Pickett > Brocher > Carroll (Worst).
- The CNN model delivered the highest V_S prediction accuracy based on supervised learning using data records from wells MN#163 and MN#225 (RMSE = 0.0456 km/s; $R^2 = 0.9808$ when applied to all 6622 data records).
- The hybrid machine learning algorithms MELM-PSO and MELM-GA, also provided highly credible V_S predictions RMSE = 0.05 to 0.06 km/s; $R^2 \sim 0.96$ when applied to all 6622 data records), whereas the empirical model achieved V_S prediction accuracy of RMSE > 0.11 km/s and $R^2 < 0.87$.
- Applying the trained and validated CNN model to the previously unseen 2072 data records from the Asmari reservoir penetrated by well MN#179 achieved V_S prediction accuracy of RMSE = 0.068 km/s and $R^2 = 0.97$.
- This impressive prediction performance confirms that the CNN model trained with supervised data from two wells can be applied to accurately predict V_S in other Asmari reservoir sections in the Marun oil field from basic well log variables where V_S logs have not been recorded.
- Properly trained deep learning and hybrid machine learning models, such as those evaluated, offer a better method of predicting V_S from multiple well-log variables, in a supervised context and with data previously unseen by the trained and validated models, than the commonly used empirical models based solely on V_P data.

Acknowledgements This research was supported by the Tomsk Polytechnic University development program.

Funding No specific funding has been received for this study.

Data availability Since the data used in the study are confidential, the authors cannot share them publicly.

Declarations

Conflict of interest The authors declare that they have no known competing financial interests or personal relationships that could have appeared to influence the work reported in this paper.

References

Abad ARB et al (2022) Robust hybrid machine learning algorithms for gas flow rates prediction through wellhead chokes in gas condensate fields. Fuel 308:121872. https://doi.org/10.1016/j.fuel.2021.121872

Abad ARB et al (2021a) Hybrid machine learning algorithms to predict condensate viscosity in the near wellbore regions of gas condensate reservoirs. Journal of Natural Gas Science and Engineering 95:104210. https://doi.org/10.1016/j.jngse.2021.104210

Abad ARB et al (2021b) Predicting oil flow rate through orifice plate with robust machine learning algorithms. Flow Meas Instrum 81:102047. https://doi.org/10.1016/j.flowmeasinst.2021.102047

Abdali, M.R., et al. (2021). Petroleum well blowouts as a threat to drilling operation and wellbore sustainability: causes, prevention, safety and emergency response. Journal of Construction Materials| Special Issue on Sustainable Petroleum Engineering ISSN 2652, 3752. doi:

Ahmadi MH et al (2020) Evaluation of electrical efficiency of photovoltaic thermal solar collector. Engineering Applications of Computational Fluid Mechanics 14:545–565. https://doi.org/10.1080/19942060.2020.1734094

Akbarpour M, Abdideh M (2020) Wellbore stability analysis based on geomechanical modeling using finite element method. Modeling

Earth Systems and Environment 6:617–626. https://doi.org/10.1007/s40808-020-00716-x
Akhundi H et al (2014) Prediction of shear wave velocity using artificial neural network technique, multiple regression and petrophysical data: A case study in Asmari reservoir (SW Iran). Open Journal of Geology. https://doi.org/10.4236/ojg.2014.47023
Al-Dousari M et al (2016) Investigating the dependence of shear wave velocity on petrophysical parameters. J Petrol Sci Eng 146:286–296. https://doi.org/10.1016/j.petrol.2016.04.036
Ali M et al (2021) Machine learning-A novel approach of well logs similarity based on synchronization measures to predict shear sonic logs. J Petrol Sci Eng 203:108602. https://doi.org/10.1016/j.petrol.2021.108602
Alkinani, H.H., et al. (2019). Intelligent data-driven analytics to predict shear wave velocity in carbonate formations: comparison between recurrent and conventional neural networks. OnePetro. https://onepetro.org/conference-paper/ARMA-2019-0511.
Asadi E et al (2019) Groundwater quality assessment for sustainable drinking and irrigation. Sustainability 12:177. https://doi.org/10.3390/su12010177
Ashraf U et al (2021) A core logging, machine learning and geostatistical modeling interactive approach for subsurface imaging of lenticular geobodies in a clastic depositional system, SE Pakistan. Nat Resour Res 30:2807–2830. https://doi.org/10.1007/s11053-021-09849-x
Ashraf U et al (2020) Application of unconventional seismic attributes and unsupervised machine learning for the identification of fault and fracture network. Appl Sci 10:3864. https://doi.org/10.3390/app10113864
Asoodeh, M., Bagheripour, P. (2012). Prediction of compressional, shear, and stoneley wave velocities from conventional well log data using a committee machine with intelligent systems. Rock mechanics and rock engineering 45, 45–63. https://doi.org/10.1007/s00603-011-0181-2.
Asoodeh, M., Bagheripour, P. (2013). Neuro-fuzzy reaping of shear wave velocity correlations derived by hybrid genetic algorithm-pattern search technique. Open Geosciences 5, 272–284. https://doi.org/10.2478/s13533-012-0129-4.
Asoodeh M, Bagheripour P (2014) ACE stimulated neural network for shear wave velocity determination from well logs. J Appl Geophys 107:102–107. https://doi.org/10.1016/j.jappgeo.2014.05.014
Azadpour M et al (2020) Rock physics model-based prediction of shear wave velocity utilizing machine learning technique for a carbonate reservoir, southwest Iran. J Petrol Sci Eng 195:107864. https://doi.org/10.1016/j.petrol.2020.107864
Bagheripour P et al (2015) Support vector regression based determination of shear wave velocity. J Petrol Sci Eng 125:95–99. https://doi.org/10.1016/j.petrol.2014.11.025
Bailey, T., Dutton, D. (2012). An empirical vp/vs shale trend for the kimmeridge clay of the central North Sea. European Association of Geoscientists & Engineers, pp. cp-293. https://doi.org/10.3997/2214-4609.20148426.
Band SS et al (2020a) Flash flood susceptibility modeling using new approaches of hybrid and ensemble tree-based machine learning algorithms. Remote Sensing 12:3568. https://doi.org/10.3390/rs12213568
Band SS et al (2020b) Novel ensemble approach of deep learning neural network (DLNN) model and particle swarm optimization (PSO) algorithm for prediction of gully erosion susceptibility. Sensors 20:5609. https://doi.org/10.3390/s20195609
Barjouei HS et al (2021) Prediction performance advantages of deep machine learning algorithms for two-phase flow rates through wellhead chokes. Journal of Petroleum Exploration and Production 11:1233–1261. https://doi.org/10.1007/s13202-021-01087-4
Bazyrov I et al (2017) Time-dependent hydro-geomechanical reservoir simulation of field production. Procedia Structural Integrity 6:228–235. https://doi.org/10.1016/j.prostr.2017.11.035
Behnia D et al (2017) Modeling of shear wave velocity in limestone by soft computing methods. Int J Min Sci Technol 27:423–430. https://doi.org/10.1016/j.ijmst.2017.03.006
Brocher TM (2005) Empirical relations between elastic wavespeeds and density in the Earth's crust. Bull Seismol Soc Am 95:2081–2092. https://doi.org/10.1785/0120050077
Castagna, J.P., et al. (1985). Relationships between compressional-wave in elastic silicate rocks and shear-wave velocities. Geophysics 50, 571–581. doi:
Cheng J, Xiong Y (2017) Application of extreme learning machine combination model for dam displacement prediction. Procedia Computer Science 107:373–378. https://doi.org/10.1016/j.procs.2017.03.120
Choubin B et al (2019) Earth fissure hazard prediction using machine learning models. Environ Res 179:108770. https://doi.org/10.1016/j.envres.2019.108770
Coello, C.C., et al. (2007). Evolutionary algorithms for solving multi-objective problems: Springer Science & Business Media. https://link.springer.com/book/10.1007%2F978-0-387-36797-2.
Darvishpour A et al (2019) Wellbore stability analysis to determine the safe mud weight window for sandstone layers. Pet Explor Dev 46:1031–1038. https://doi.org/10.1016/S1876-3804(19)60260-0
Dehghani M et al (2020) Spatial analysis of seasonal precipitation over Iran: Co-variation with climate indices. ISPRS Int J Geo Inf 9:73. https://doi.org/10.3390/ijgi9020073
Dusseault MB (2011) Geomechanical challenges in petroleum reservoir exploitation. KSCE J Civ Eng 15:669–678. https://doi.org/10.1007/s12205-011-0007-5
Eberhart-Phillips D et al (1989) Empirical relationships among seismic velocity, effective pressure, porosity, and clay content in sandstone. Geophysics 54:82–89. https://doi.org/10.1190/1.1442580
Ebrahimi A et al (2022) Estimation of shear wave velocity in an Iranian oil reservoir using machine learning methods. J Petrol Sci Eng 209:109841. https://doi.org/10.1016/j.petrol.2021.109841
Emadi M et al (2020) Predicting and mapping of soil organic carbon using machine learning algorithms in Northern Iran. Remote Sensing 12:2234. https://doi.org/10.3390/rs12142234
Eskandari, H., et al. (2004). Application of multiple regression and artificial neural network techniques to predict shear wave velocity from wireline log data for a carbonate reservoir South-West Iran. CSEG recorder 42, 48. doi:
Farsi M et al (2021) Prediction of oil flow rate through orifice flow meters: Optimized machine-learning techniques. Measurement 174:108943. https://doi.org/10.1016/j.measurement.2020.108943
Farsi, M., et al. (2021b). Predicting Formation Pore-Pressure from Well-Log Data with Hybrid Machine-Learning Optimization Algorithms. Natural Resources Research, 1–27. https://doi.org/10.1007/s11053-021-09852-2.
Fourie, A., Vawda, A. (1992). The importance of a thorough geotechnical site investigation at the planning stage of urban development, 1 ed. Springer, pp. 57–72. https://doi.org/10.1007/BF03036539.
Ghalandari M et al (2019a). Aeromechanical Optimization of First Row Compressor Test Stand Blades. https://doi.org/10.20944/preprints201905.0049.v1
Ghalandari M et al (2019b) Aeromechanical optimization of first row compressor test stand blades using a hybrid machine learning model of genetic algorithm, artificial neural networks and design of experiments. Engineering Applications of Computational

Fluid Mechanics 13:892–904. https://doi.org/10.1080/19942060.2019.1649196
Gholami A et al (2020) Estimation of shear wave velocity from post-stack seismic data through committee machine with cuckoo search optimized intelligence models. J Petrol Sci Eng 189:106939. https://doi.org/10.1016/j.petrol.2020.106939
Gholami, R., et al. (2014). Shear wave velocity prediction using seismic attributes and well log data. Acta Geophysica 62, 818–848. https://doi.org/10.2478/s11600-013-0200-7
Ghorbani, H., et al. (2021). Accurate determination of shear wave velocity using LSSVM-GA algorithm based on petrophysical log, 1 ed. European Association of Geoscientists & Engineers, pp. 1–3. https://doi.org/10.3997/2214-4609.202137015.
Ghorbani H et al (2017) Prediction of gas flow rates from gas condensate reservoirs through wellhead chokes using a firefly optimization algorithm. Journal of Natural Gas Science and Engineering 45:256–271. https://doi.org/10.1016/j.jngse.2017.04.034
Ghorbani H et al (2020a) Performance comparison of bubble point pressure from oil PVT data: Several neurocomputing techniques compared. Experimental and Computational Multiphase Flow 2:225–246. https://doi.org/10.1007/s42757-019-0047-5
Ghorbani H et al (2020b) Prediction of oil flow rate through an orifice flow meter: Artificial intelligence alternatives compared. Petroleum 6:404–414. https://doi.org/10.1016/j.petlm.2018.09.003
Ghorbani H et al (2019) Predicting liquid flow-rate performance through wellhead chokes with genetic and solver optimizers: an oil field case study. Journal of Petroleum Exploration and Production Technology 9:1355–1373. https://doi.org/10.1007/s13202-018-0532-6
Ghorbani H et al (2020c) Adaptive neuro-fuzzy algorithm applied to predict and control multi-phase flow rates through wellhead chokes. Flow Meas Instrum 76:101849. https://doi.org/10.1016/j.flowmeasinst.2020.101849
Gullu, H. (2017). On the prediction of unconfined compressive strength of silty soil stabilized with bottom ash, jute and steel fibers via artificial intelligence. Geomechanics & engineering 12, 441–464. doi:
Güllü, H., Jaf, H.S. (2016). Full 3D nonlinear time history analysis of dynamic soil–structure interaction for a historical masonry arch bridge. Environmental Earth Sciences 75, 1–17. https://doi.org/10.1007/s12665-016-6230-0.
Güllü H, Karabekmez M (2017) Effect of near-fault and far-fault earthquakes on a historical masonry mosque through 3D dynamic soil-structure interaction. Eng Struct 152:465–492. https://doi.org/10.1016/j.engstruct.2017.09.031
Güllü, H., Pala, M. (2014). On the resonance effect by dynamic soil–structure interaction: a revelation study. Natural hazards 72, 827–847. https://doi.org/10.1007/s11069-014-1039-1.
Guo Z, Li X-Y (2015) Rock physics model-based prediction of shear wave velocity in the Barnett Shale formation. J Geophys Eng 12:527–534. https://doi.org/10.1088/1742-2132/12/3/527
Hazbeh O et al (2021a) Comparison of accuracy and computational performance between the machine learning algorithms for rate of penetration in directional drilling well. Petroleum Research 6:271–282. https://doi.org/10.1016/j.ptlrs.2021.02.004
Hazbeh O et al (2021b) Hybrid computing models to predict oil formation volume factor using multilayer perceptron algorithm. Journal of Petroleum and Mining Engineering 23:17–30. https://doi.org/10.21608/JPME.2021.52149.1062
Huang, G.-B. (2014). An insight into extreme learning machines: random neurons, random features and kernels. Cognitive Computation 6, 376–390. https://link.springer.com/article/10.1007%2Fs12559-014-9255-2.
Huang G-B et al (2011) Extreme learning machine for regression and multiclass classification. IEEE Transactions on Systems, Man, and Cybernetics. Part B (cybernetics) 42:513–529. https://doi.org/10.1109/TSMCB.2011.2168604
Huang G-B et al (2006) Extreme learning machine: theory and applications. Neurocomputing 70:489–501. https://doi.org/10.1016/j.neucom.2005.12.126
Hudson JA et al (2005) Guidance on numerical modelling of thermo-hydro-mechanical coupled processes for performance assessment of radioactive waste repositories. Int J Rock Mech Min Sci 42:850–870. https://doi.org/10.1016/j.ijrmms.2005.03.018
Jafarizadeh F et al (2022) Data driven models to predict pore pressure using drilling and petrophysical data. Energy Rep 8:6551–6562. https://doi.org/10.1016/j.egyr.2022.04.073
Joloudari JH et al (2020) Coronary artery disease diagnosis; ranking the significant features using a random trees model. Int J Environ Res Public Health 17:731. https://doi.org/10.3390/ijerph17030731
Jørstad A et al (1999) Model-based shear-wave velocity estimation versus empirical regressions [Link]. Geophys Prospect 47:785–797. https://doi.org/10.1046/j.1365-2478.1999.00154.x
Kalbasi R et al (2021) Finding the best station in Belgium to use residential-scale solar heating, one-year dynamic simulation with considering all system losses: economic analysis of using ETSW. Sustainable Energy Technol Assess 45:101097. https://doi.org/10.1016/j.seta.2021.101097
Kamali MZ et al (2022) Permeability prediction of heterogeneous carbonate gas condensate reservoirs applying group method of data handling. Mar Pet Geol 139:105597. https://doi.org/10.1016/j.marpetgeo.2022.105597
Khoshouei, M., Bagherpour, R. (2021). Predicting the Geomechanical Properties of Hard Rocks Using Analysis of the Acoustic and Vibration Signals During the Drilling Operation. Geotechnical and Geological Engineering 39, 2087–2099. https://doi.org/10.1007/s10706-020-01611-z.
Krizhevsky A et al (2017) ImageNet classification with deep convolutional neural networks. Commun ACM 60:84–90. https://doi.org/10.1145/3065386
Lee, M.W. (2013). Comparison of methods for predicting shear-wave velocities of unconsolidated shallow sediments in the Gulf of Mexico. US Department of the Interior, US Geological Survey Reston.
Lei X et al (2020) GIS-based machine learning algorithms for gully erosion susceptibility mapping in a semi-arid region of Iran. Remote Sensing 12:2478. https://doi.org/10.3390/rs12152478
Mahmoudi MR et al (2021) Principal component analysis to study the relations between the spread rates of COVID-19 in high risks countries. Alex Eng J 60:457–464. https://doi.org/10.1016/j.aej.2020.09.013
Maleki S et al (2014) Prediction of shear wave velocity using empirical correlations and artificial intelligence methods. NRIAG J Astron Geophys 3:70–81. https://doi.org/10.1016/j.nrjag.2014.05.001
Medetbekova M et al (2021) High pressure jet drilling effect in chalk and alteration of local geomechanics properties surrounding the radial hole. Int J Mech Sci 191:105954. https://doi.org/10.1016/j.ijmecsci.2020.105954
Mehrgini, B., et al. (2019). Shear wave velocity prediction using Elman artificial neural network. Carbonates and Evaporites 34, 1281–1291. https://doi.org/10.1007/s13146-017-0406-x.
Miah MI (2021) Improved prediction of shear wave velocity for clastic sedimentary rocks using hybrid model with core data. Journal of Rock Mechanics and Geotechnical Engineering 13:1466–1477. https://doi.org/10.1016/j.jrmge.2021.06.014
Miah MI et al (2021) Model development for shear sonic velocity using geophysical log data: Sensitivity analysis and statistical assessment. Journal of Natural Gas Science and Engineering 88:103778. https://doi.org/10.1016/j.jngse.2020.103778

Mohamadian, N., et al. (2022). Carbon-nanotube-polymer nanocomposites enable wellbore cements to better inhibit gas migration and enhance sustainability of natural gas reservoirs, Sustainable Natural Gas Reservoir and Production Engineering. Elsevier, pp. 243–268.

Mohamadian N et al (2021) A geomechanical approach to casing collapse prediction in oil and gas wells aided by machine learning. J Petrol Sci Eng 196:107811. https://doi.org/10.1016/j.petrol.2020.107811

Mosavi A et al (2020) Comprehensive review of deep reinforcement learning methods and applications in economics. Mathematics 8:1640. https://doi.org/10.3390/math8101640

Mosavi A, Safaei-Farouji M (2021) Oil Family Typing Using a Hybrid Model of Self-Organizing Map and Artificial Neural Network. Available at SSRN. https://doi.org/10.2139/ssrn.3991002

Mousavi SM et al (2021) Deep learning for wave energy converter modeling using long short-term memory. Mathematics 9:871. https://doi.org/10.3390/math9080871

Nabipour M et al (2020) Deep learning for stock market prediction. Entropy 22:840. https://doi.org/10.3390/e22080840

Naveshki M et al (2021) Prediction of bubble point pressure using new hybrid computationail intelligence models. Journal of Chemical and Petroleum Engineering 55:203–222. https://doi.org/10.22059/JCHPE.2021.314719.1341

Ojha, M., Sain, K. (2014). Velocity-porosity and velocity-density relationship for shallow sediments in the Kerala-Konkan basin of western Indian margin. Journal of the Geological Society of India 84, 187–191. https://doi.org/10.1007/s12594-014-0122-2.

Olayiwola T, Sanuade OA (2021) A data-driven approach to predict compressional and shear wave velocities in reservoir rocks. Petroleum 7:199–208. https://doi.org/10.1016/j.petlm.2020.07.008

Olayiwola T et al (2021) Evolving strategies for shear wave velocity estimation: smart and ensemble modeling approach. Neural Comput Appl 33:17147–17159. https://doi.org/10.1007/s00521-021-06306-x

Oloruntobi O, Butt S (2020) The shear-wave velocity prediction for sedimentary rocks. Journal of Natural Gas Science and Engineering 76:103084. https://doi.org/10.1016/j.jngse.2019.103084

Oloruntobi O et al (2019) Data-driven shear wave velocity prediction model for siliciclastic rocks. J Petrol Sci Eng 183:106293. https://doi.org/10.1016/j.petrol.2019.106293

Pedersen MEH, Chipperfield AJ (2010) Simplifying particle swarm optimization. Appl Soft Comput 10:618–628. https://doi.org/10.1016/j.asoc.2009.08.029

Pickett GR (1963) Acoustic character logs and their applications in formation evaluation. J Petrol Technol 15:659–667. https://doi.org/10.2118/452-PA

Rajabi M et al (2021) Novel hybrid machine learning optimizer algorithms to prediction of fracture density by petrophysical data. Journal of Petroleum Exploration and Production Technology 11:4375–4397. https://doi.org/10.1007/s13202-021-01321-z

Rajabi M et al (2010) Intelligent approaches for prediction of compressional, shear and Stoneley wave velocities from conventional well log data: A case study from the Sarvak carbonate reservoir in the Abadan Plain (Southwestern Iran). Comput Geosci 36:647–664. https://doi.org/10.1016/j.cageo.2009.09.008

Rajabi M et al (2022a) Prediction of Shear Wave Velocity by Extreme Learning Machine Technique from Well Log Data. Journal of Petroleum Geomechanics 4:18–35. https://doi.org/10.22107/JPG.2022.298520.1151

Rajabi M et al (2022b) Sensitivity analysis of effective factors for estimating formation pore pressure using a new method: the LSSVM-PSO algorithm. Journal of Petroleum Geomechanics 4:19–39. https://doi.org/10.22107/JPG.2022.298551.1152

Ranaee E et al (2021) Analysis of the performance of a crude-oil desalting system based on historical data. Fuel 291:120046. https://doi.org/10.1016/j.fuel.2020.120046

Rashidi S et al (2021) Determination of bubble point pressure & oil formation volume factor of crude oils applying multiple hidden layers extreme learning machine algorithms. J Petrol Sci Eng 202:108425. https://doi.org/10.1016/j.petrol.2021.108425

Rashidi S et al (2020) Shear modulus prediction of embedded pressurized salt layers and pinpointing zones at risk of casing collapse in oil and gas wells. J Appl Geophys 183:104205. https://doi.org/10.1016/j.jappgeo.2020.104205

Rezaee MR et al (2007) Prediction of shear wave velocity from petrophysical data utilizing intelligent systems: An example from a sandstone reservoir of Carnarvon Basin, Australia. J Petrol Sci Eng 55:201–212. https://doi.org/10.1016/j.petrol.2006.08.008

Rezakazemi M et al (2019) ANFIS pattern for molecular membranes separation optimization. J Mol Liq 274:470–476. https://doi.org/10.1016/j.molliq.2018.11.017

Rhett, D.W. (1998). Ekofisk revisited: a new model of Ekofisk reservoir geomechanical behavior. OnePetro. https://onepetro.org/conference-paper/SPE-47273-MS.

Sadeghzadeh M et al (2020) Prediction of thermo-physical properties of TiO2-Al2O3/water nanoparticles by using artificial neural network. Nanomaterials 10:697. https://doi.org/10.3390/nano10040697

Seifi A et al (2020) Modeling and uncertainty analysis of groundwater level using six evolutionary optimization algorithms hybridized with ANFIS, SVM, and ANN. Sustainability 12:4023. https://doi.org/10.3390/su12104023

Shabani S et al (2020) Modeling pan evaporation using Gaussian process regression K-nearest neighbors random forest and support vector machines; comparative analysis. Atmosphere 11:66. https://doi.org/10.3390/atmos11010066

Shamshirband S et al (2020) Prediction of significant wave height; comparison between nested grid numerical model, and machine learning models of artificial neural networks, extreme learning and support vector machines. Engineering Applications of Computational Fluid Mechanics 14:805–817. https://doi.org/10.1080/19942060.2020.1773932

Shamsirband, S., Mehri Khansari, N. (2021). Micro-mechanical damage diagnosis methodologies based on machine learning and deep learning models. Journal of Zhejiang University-SCIENCE A 22, 585–608. https://doi.org/10.1631/jzus.A2000408.

Shiroodi SK et al (2017) Shear wave prediction using committee fuzzy model constrained by lithofacies, Zagros basin, SW Iran. J Afr Earth Sc 126:123–135. https://doi.org/10.1016/j.jafrearsci.2016.11.016

Silver, D., et al. (2016). Mastering the game of Go with deep neural networks and tree search. nature 529, 484–489. https://doi.org/10.1038/nature16961.

Singh, S., Kanli, A.I. (2016). Estimating shear wave velocities in oil fields: a neural network approach. Geosciences Journal 20, 221–228. https://link.springer.com/article/10.1007%2Fs12303-015-0036-z.

Sohail GM et al (2020) An integrated petrophysical and geomechanical characterization of Sembar Shale in the Lower Indus Basin, Pakistan, using well logs and seismic data. Journal of Natural Gas Science and Engineering 78:103327. https://doi.org/10.1016/j.jngse.2020.103327

Stark, N., et al. (2014). Cost-effective geotechnical and sedimentological early site assessment for ocean renewable energies. IEEE, pp. 1–8. https://doi.org/10.1109/OCEANS.2014.7003004.

Sun, F.-l., et al. (2008). An S-Wave Velocity Predicted Method [J]. Progress in Geophysics 2. https://en.cnki.com.cn/Article_en/CJFDTotal-DQWJ200802023.htm.

Taherei Ghazvinei P et al (2018) Sugarcane growth prediction based on meteorological parameters using extreme learning machine and artificial neural network. Engineering Applications of Computational Fluid Mechanics 12:738–749. https://doi.org/10.1080/19942060.2018.1526119

Thanh HV et al (2022) Knowledge-based machine learning techniques for accurate prediction of CO2 storage performance in

underground saline aquifers. Appl Energy 314:118985. https://doi.org/10.1016/j.apenergy.2022.118985
Tokeshi K et al (2013) Use of surface waves for geotechnical engineering applications in Western Sydney. Adv Geosci 35:37–44. https://doi.org/10.5194/adgeo-35-37-2013
Vo-Thanh H et al (2022) Robust machine learning models of carbon dioxide trapping indexes at geological storage sites. Fuel 316:123391. https://doi.org/10.1016/j.fuel.2022.123391
Vo Thanh H et al (2020) Application of artificial neural network for predicting the performance of CO2 enhanced oil recovery and storage in residual oil zones. Sci Rep 10:1–16. https://doi.org/10.1038/s41598-020-73931-2
Wang J et al (2020) Shear wave velocity prediction based on adaptive particle swarm optimization optimized recurrent neural network. J Petrol Sci Eng 194:107466. https://doi.org/10.1016/j.petrol.2020.107466
Wang, J., et al. (2019). An effective method for shear-wave velocity prediction in sandstones. Marine Geophysical Research 40, 655–664. https://doi.org/10.1007/s11001-019-09396-4.
Wang, S.-J., et al. (2014). Face recognition and micro-expression recognition based on discriminant tensor subspace analysis plus extreme learning machine. Neural processing letters 39, 25–43. https://link.springer.com/article/10.1007%2Fs11063-013-9288-7.
Weijun, N., et al. (2017). Prediction of shear wave velocity in shale reservoir based on logging data and machine learning. IEEE, pp. 231–234. https://doi.org/10.1109/ICKEA.2017.8169935.
Wood DA (2020) Bakken stratigraphic and type well log learning network exploited to predict and data mine shear wave acoustic velocity. J Appl Geophys 173:103936. https://doi.org/10.1016/j.jappgeo.2019.103936
Xu S, White RE (1995) A new velocity model for clay-sand mixtures 1. Geophys Prospect 43:91–118. https://doi.org/10.1111/j.1365-2478.1995.tb00126.x
Yeom C-U, Kwak K-C (2017) Short-term electricity-load forecasting using a TSK-based extreme learning machine with knowledge representation. Energies 10:1613. https://doi.org/10.3390/en10101613
Yu, A.W., et al. (2018). Qanet: Combining local convolution with global self-attention for reading comprehension. arXiv preprint arXiv:1804.09541. https://arxiv.org/abs/1804.09541.
Zhang G et al (2022) A robust approach to pore pressure prediction applying petrophysical log data aided by machine learning techniques. Energy Rep 8:2233–2247. https://doi.org/10.1016/j.egyr.2022.01.012
Zhang, G.Z., et al. (2012). A shear velocity estimation method for carbonate rocks based on the improved Xu-White model: Oil Geophysical Prospecting. https://www.scopus.com/record/display.uri?eid=2-s2.0-84869116773&origin=inward#references.
Zhang Y et al (2021) The adoption of deep neural network (DNN) to the prediction of soil liquefaction based on shear wave velocity. Bull Eng Geol Env 80:5053–5060. https://doi.org/10.1007/s10064-021-02250-1
Zhang Y et al (2020) Improvement of petrophysical workflow for shear wave velocity prediction based on machine learning methods for complex carbonate reservoirs. J Petrol Sci Eng 192:107234. https://doi.org/10.1016/j.petrol.2020.107234
Zhong, C., et al. (2021). Shear Wave Velocity Prediction of Carbonate Reservoirs Based on CatBoost. IEEE, pp. 622–626. https://doi.org/10.1109/ICAIBD51990.2021.9459061.

Authors and Affiliations

Meysam Rajabi[1] · Omid Hazbeh[2] · Shadfar Davoodi[3] · David A. Wood[4] · Pezhman Soltani Tehrani[5] · Hamzeh Ghorbani[6] · Mohammad Mehrad[7] · Nima Mohamadian[8] · Valeriy S. Rukavishnikov[3] · Ahmed E. Radwan[10]

Meysam Rajabi
m.rajabi@birjandut.ac.ir

Omid Hazbeh
omid-hazbeh@stu.scu.ac.ir

Shadfar Davoodi
davoodis@hw.tpu.ru

David A. Wood
dw@dwasolutions.com

Pezhman Soltani Tehrani
p.soltani.tehrani@ut.ac.ir

Mohammad Mehrad
mmehrad1986@gmail.com

Nima Mohamadian
nima.0691@gmail.com

Valeriy S. Rukavishnikov
rukavishnikovvs@hw.tpu.ru

Ahmed E. Radwan
radwanae@yahoo.com

[1] Department of Mining Engineering, Birjand University of Technology, Birjand, Iran

[2] Faculty of Earth Sciences, Shahid Chamran University, Ahwaz, Iran

[3] School of Earth Sciences & Engineering, Tomsk Polytechnic University, Lenin Avenue, Tomsk, Russia

[4] DWA Energy Limited, Lincoln LN5 9JP, UK

[5] Department of Petroleum Engineering, University of Tehran, Kish International Campus, Kish, Iran

[6] Young Researchers and Elite Club, Ahvaz Branch, Islamic Azad University, Ahvaz, Iran

[7] Faculty of Mining, Petroleum and Geophysics Engineering, Shahrood University of Technology, Shahrood, Iran

[8] Young Researchers and Elite Club, Omidiyeh Branch, Islamic Azad University, Omidiyeh, Iran

[10] Faculty of Geography and Geology, Institute of Geological Sciences, Jagiellonian University, Gronostajowa 3a; 30-387, Kraków, Poland